Endothelial Rap1B mediates T-cell exclusion to promote tumor growth – a novel mechanism underlying vascular immunosuppression

Running title: Endothelial Rap1B mediates VEGF immunosuppression

Guru Prasad Sharma[a], Ramoji Kosuru[a], Sribalaji Lakshmikanthan[a], Shikan Zheng[a], Yao Chen[a, b], Robert Burns[a], Gang Xin[a], Weiguo Cui[a, b], W. and Magdalena Chrzanowska[a, c, d].

[a]Blood Research Institute, Versiti, Milwaukee, Wisconsin
[b]Department of Microbiology and Immunology, Medical College of Wisconsin, Milwaukee, Wisconsin
[c]Department of Pharmacology and Toxicology, Medical College of Wisconsin, Milwaukee, Wisconsin
[d]Cardiovascular Center, Medical College of Wisconsin, Milwaukee, Wisconsin

Keywords: tumor microenvironment, tumor blood vessels, vascular anergy, small GTPase Rap1, angiogenic signaling

Financial support: This work was funded by NIH grant R01HL111582 (M.C.). W.C. is supported by American Cancer Society Research Scholar Grant. RK is supported by the Director's Fellowship Award at the Blood Research Institute of Versiti, Wisconsin.

Corresponding Author:
Magdalena Chrzanowska
ORCID id: 0000-0003-4182-2126
Blood Research Institute, Versiti, Milwaukee, Wisconsin 53201-2178
Department of Pharmacology and Toxicology, Medical College of Wisconsin, Milwaukee, Wisconsin 53226
tel: 414.937.3890
email: mchrzanowska@versiti.org

Conflict of interest disclosure: The authors declare no potential conflicts of interest.

Abstract

Overcoming vascular immunosuppression: lack of endothelial cell (EC) responsiveness to inflammatory stimuli in the proangiogenic environment of tumors, is essential for successful cancer immunotherapy. The mechanisms through which Vascular Endothelial Growth Factor (VEGF) modulates tumor EC response to exclude T cells are not well understood. The goal was to determine the role of EC Rap1B, a small GTPase that positively regulates VEGF-angiogenesis during development, in tumor growth in vivo. Using mouse models of Rap1B deficiency, $Rap1B^{+/-}$ and EC-specific Rap1B KO ($Rap1B^{i\Delta EC}$) we demonstrate that EC Rap1B restricts tumor growth and angiogenesis. More importantly, EC-specific Rap1B deletion leads to an altered tumor microenvironment with increased recruitment of leukocytes and increased activity of tumor $CD8^+$ T cells. We find that tumor growth, albeit not angiogenesis, is restored in $Rap1B^{i\Delta EC}$ mice by depleting $CD8^+$ T cells. Mechanistically, global transcriptome analysis indicated upregulation of the tumor cytokine, TNF-α, -induced signaling and NFκB transcriptional activity in Rap1B-deficient ECs. Functionally, EC Rap1B deletion led to upregulation of NFκB activity and enhanced Cell Adhesion Molecules (CAMs) expression in TNF-α stimulated ECs. Importantly, CAM expression was upregulated also in tumor ECs from $Rap1B^{i\Delta EC}$ mice, vs. controls. Significantly, deletion of Rap1B abrogated VEGF immunosuppressive downregulation of CAM expression, demonstrating that Rap1B is essential for VEGF-suppressive signaling. Thus, our studies identify a novel endothelial-endogenous mechanism underlying VEGF-dependent desensitization of EC to pro-inflammatory stimuli. Significantly, they identify EC Rap1 as a potential novel vascular target in cancer immunotherapy.

Introduction

Recent cancer immunotherapies involving immune checkpoint inhibitors and chimeric antigen receptor (CAR)-T cell transfer show promise for cancer treatments. These treatments exploit the complex interactions between cancer cells and host tissue in tumor microenvironment (TME), which determine tumor growth and metastasis. Understanding the mechanisms of the host immune response to the tumor is, therefore, critical to the success of immunotherapy (Hendry et al., 2016).

Tumor vasculature is a key component of the TME. In response to hypoxia and proangiogenic cytokines, endothelial cell (EC)-driven angiogenesis gives rise to vessels that supply blood to feed the tumor. Moreover, tumor ECs control the TME by regulating leukocyte trafficking and modulating the immune response. The density of tumor-infiltrating T cells, and, in particular, $CD8^+$ cytotoxic T cells, correlates with improved survival in many tumors (Fridman et al., 2012). Thus, the success of adoptive T-cell therapies to treat solid cancers depends on successful homing and infiltration by T-lymphocytes (Ager et al., 2016).

Endothelial cells control leukocyte trafficking by upregulating ligands for T-cell adhesion, among them Cell Adhesion Molecules (CAMs): VCAM-1 and ICAM-1, as a response to the proinflammatory cytokines in the TME (Ley et al., 2007). While essential for leukocyte recruitment, the proangiogenic environment in tumors dampens this response. Clinical data and experimental studies in mice suggest that tumor blood vessels are anergic to inflammatory stimuli and the recruitment of cytotoxic $CD8^+$ T cells (Ager et al., 2016; Joyce and Fearon, 2015), as demonstrated in a number of tumors, including melanoma (Hendry et al., 2016). Endothelial anergy – lack of responsiveness to inflammatory stimuli (Griffioen et al., 1996) is, in part, due to elevated angiogenic factors. In particular, VEGF-A from various TME components is upregulated in solid tumors (VEGF expression correlates with poor prognosis). VEGF decreases EC responsiveness to proinflammatory cytokines and proinflammatory adhesion receptor expression, suppressing leukocyte recruitment (Piali et al., 1995). Specifically, VEGF blocks TNF-a induced NF-kB required for CAM expression and T-cell infiltration (Huang et al., 2015). This concept is supported by evidence from anti-angiogenic therapies leading to upregulation of adhesion molecules on tumor vasculature and increased leukocyte infiltration (Dirkx et al., 2006; Hendry et al., 2016). Interference with VEGF signaling normalizes tumor vasculature and restores responsiveness of ECs to adoptive T-cell therapy also in melanoma (Shrimali et al., 2010). However, incomplete understanding of the mechanisms through which VEGF modulates tumor EC response to exclude T cells (cytokine-induced CAM expression), constitutes a major obstacle in overcoming immunosuppressive properties of tumor ECs.

Two closely related isoforms of a ubiquitously expressed small GTPase Rap1, Rap1A and Rap1B, are best known for modulation of adhesive and signaling properties of integrins and cadherins (Boettner and Van Aelst, 2009). In endothelium, Rap1 isoforms are required for vessel stabilization during development, but are not essential for vessel maintenance after birth. Instead, both isoforms are positive regulators of developmental angiogenesis (Carmona et al., 2009; Chrzanowska-Wodnicka et al., 2008; Yan et al., 2008). In particular, Rap1B, the predominant Rap1 isoform in the endothelium, promotes VEGF-induced VEGFR2 activation and signaling and its deficiency impairs VEGF-induced angiogenic responses (Chrzanowska-Wodnicka, 2010). Interestingly, Rap1B is also essential for normal VEGF-induced EC barrier dissolution and its deficiency prevents VEGF-mediated hyperpermeability in a diabetes model in vivo (Lakshmikanthan et al., 2018). Thus, there exist synergy between Rap1 and VEGF signaling. However, the role of Rap1B in tumor vasculature has not been studied and its involvement in mechanisms through which VEGF modulates tumor EC responses is unknown.

In this study our goal was to determine whether endothelial Rap1B regulated tumor growth in vivo. We hypothesized that Rap1B deficiency would lead to impaired tumor growth by restricting angiogenesis. We found that, beyond restriction of vessel growth, endothelial Rap1B deficiency led to increased leukocyte recruitment and leukocyte activation. Unexpectedly, deletion of $CD8^+$ T cells rescued impaired tumor growth in EC-specific Rap1B knockout mice ($Rap1B^{i\Delta EC}$), without normalizing endothelial cell number. At the molecular level, Rap1B deficiency increased EC responsiveness to TME-associated cytokine, TNFα, leading to increased T-cell adhesion. Transcriptomic analysis indicated the significant upregulation of TNFα signaling pathways and NFκB transcription, including proinflammatory CAM expression. Importantly, CAM expression was upregulated in tumor ECs from $Rap1B^{i\Delta EC}$ mice. Strikingly, Rap1-deficiency prevented the VEGF-induced inhibition of ECs' proinflammatory response. Our results demonstrate that Rap1B plays an important role in VEGF modulation of EC response in TME, acting predominantly as a suppressor of proinflammatory response. Our findings also suggest inhibition of endothelial Rap1B signaling as a novel target in overcoming endothelial anergy in tumor therapy.

Materials and Methods

In vivo mouse tumor model

All mouse procedures were performed according to the protocol approved by Medical College of Wisconsin Institutional Animal Use and Care Committee. Generation of total Rap1B knockout (*Rap1B*$^{-/-}$) mice and endothelial cell (EC)-specific Rap1B-knockout mice (Cdh5(PAC)-

CreERT2$^{+/0}$; Rap1A$^{+/+}$ Rap1B$^{f/f}$; Rap1B$^{i\Delta EC}$) has been previously described (Chrzanowska-Wodnicka et al., 2005; Lakshmikanthan et al., 2015). Global *Rap1B* gene heterozygous mice (*Rap1B*$^{+/-}$*;* C57Bl/6), in which Rap1B expression is decreased to ~50% of *Rap1B*$^{+/+}$ (WT, control mice), generated by crossing male *Rap1B*$^{-/-}$ and female WT mice used for analysis of Rap1B-deficiency on tumor growth because of high degree of lethality of total Rap1B knockout mice (*Rap1B*$^{-/-}$*).* Cdh5-Cre-negative mice, or mice injected with carrier oil only were used as controls for Rap1B$^{i\Delta EC}$ mice. Both males and females between the ages of 8 and 20 weeks were used in the study. Melanoma tumors were developed with subcutaneously implanted B16F10 cells (2 × 10^5 in 100µl PBS) into the flank area. Tumor growth was monitored using microcallipers every other day for till harvest on day 15th, when mice were killed, tumors isolated, weighed and processed for flow cytometry analysis. For CD8$^+$-T cell depletion, tumor bearing mice were treated with purified anti-mouse CD8 mAb (clone 53-6.7), or control mAb (clone 2A3) injected itraperitoneally to mice on days 0, 2 and 9 (Figure 3A). The efficiency of CD8$^+$ T cell depletion was determined in tumors, blood, bone marrow and spleen by flow cytometry and by hematological analysis.

Cell lines and treatments

All cells lines were obtained from ATCC. B16F10 mouse melanoma cells were cultured in Roswell Park Memorial Institute (RPMI) medium supplemented with 0.1 mM nonessential amino acids, 1 mM sodium pyruvate, 2 mM l-glutamine, 25 mM HEPES, 55 µM 2-mercaptoethanol, 10% FCS and 1% penicillin-streptomycin (100 U/ml penicillin and 100 µg/ml streptomycin). Human umbilical vein endothelial cells (HUVEC) cultured in endothelial growth medium (EGM-2, Lonza, UK) for fewer than 5 passages were used in all experiments. Human T cell leukemia cell line, Jurkat E6–1, were cultured in RPMI media supplemented with 10% FCS and 1% penicillin-streptomycin. All cells were maintained in a humidified 5% CO_2 incubator at 37 °C. 40-50% confluent HUVEC monolayers were transfected with 50nM Rap1B siGENOME siRNA pool or with non-targeting siRNA pool (Dharmacon) for 6h in OPTIMEM, and cultured for an additional 30 hours in a complete EBM culture medium. Knockdown efficiency was assessed by Western blotting. For T-cell adhesion assay, RNA sequencing and analysis of CAM expression, siRap1B or siControl-transfected HUVECs were treated with 50nM TNF-α (2% FBS EBM basal medium) for 12 hrs, prior to lysis as described below. For analysis of VEGF-induced suppression of CAM expression, cells were simultaneously treated with 50 ng/ml VEGF, as previously described (Huang et al., 2015).

Tumor cell analysis by flow cytometry

Single-cell suspensions of tumors and peripheral organs were prepared in flow cytometry staining buffer (2% FCS + 1 mM EDTA in PBS), as follows. Tumors were digested in RPMI 1640 (Lonza) supplemented with 0.6 mg ml^{-1} collagenase type I (Worthington 4196), 0.1 mg ml^{-1} Type IV bovine pancreatic DNase (Sigma-Aldrich) and 1M $MgCl_2$ (Sigma) for 45 min at 37 °C, passed through a 70 µm cell strainer and subjected to red blood cell lysis and filtration. A single-cell suspension of the spleen was obtained by tissue mincing in staining buffer. Bone Marrow (BM) cells were isolated by flushing femur and tibia bones in staining buffer and filtering through a 70µm nylon mesh. Peripheal blood monocytic cells (PBMCs) from whole blood were isolated by Histopaque gradient method. RBCs were removed using ACK lysis buffer (Lonza). The equal number of cells for each sample were stained with specific directly conjugated monoclonal antibodies (Supplemental Table 1), as previously described (Xin et al., 2020). Controls were stained with IgG isotype-matched control mAbs. 7-AAD dye (Sigma) was used to differentiate live and dead cells. Intracellular granzyme B and INFγ staining was performed in cells that had fixed and permeabilized in Flow Cytometry Fixation and Permeabilization Buffers (Catalog numbers FC004, FC005, R&D systems) following manufacturer's protocol. Stained samples were analyzed on an LSR II flow cytometer (BD Biosciences) or MACSQuant Analyzer 10 (Miltenyi). The compensation was set up for all the colors used in the experiment. Data were analyzed with the FlowJo software (FlowJo LLC, version 10.0.7). Cellular debris and doublets were removed using viability dye and FSC-A FSC-H gating.

RNA sequencing

siRap1B- or siControl-transfected HUVECs, cultured in growth media (EGM-2, Lonza) were treated with TNF-α for 12 hours. For each biological replicate RNA was extracted from 3 x 10^5 cells grown in parallel dishes using TRIzol™ reagent. RNA quantity and quality were assessed by Agilent high sensitivity RNA-Tape Station. RNA-seq libraries were prepared using a modified SMART-Seq2 protocol (Picelli et al., 2014) and sequenced on Illumina NextSeq 500 sequencer using a high-output V2 75 cycle kit (Illumina) in 37 bp paired-end mode. Reads were pseudo-aligned to the human transcriptome (Ensembl GRCh38 release 102) and expression was quantified using Salmon v1.3.0 (Patro et al., 2017). DESeq2 v 1.26.0 Wald tests were used to determine whether gene expression fold changes were significantly different from zero (Love et al., 2014). For heatmap visualization, data were transformed using the regularized logarithmic transformation (Love et al., 2014). Pre-ranked gene set enrichment analyses (GSEA) were conducted using DESeq2 shrunken fold-changes and fgsea v1.12.0. The KEGG (Ogata et al.,

1999), Reactome (Fabregat et al., 2018) and MSigDB C3:TFT (transcription factor targets) (Liberzon et al., 2011) databases were used for GSEA (Subramanian et al., 2005). The Benjamini-Hochberg method was used to adjust p-values for false-discovery in both differential expression and GSEA analysis (Benjamini and Hochberg, 1995). Data were deposited within NCBI GEO, Accession ID: GSE186046.

NFκB activity assay

HUVECs were plated onto 6-well plates at a density of 5×10^5 cells/well and transfected with 50 nM Rap1B siGENOME siRNA pool or with non-targeting siRNA pool (Dharmacon) for 6 hr in OPTIMEM, and cultured for an additional 18 hr in a complete EBM culture medium. After 24 hr, siControl and siRap1B cells were infected with NFκB reporter construct pNL3.2.NFκB-RE[NlucP/NF-κB-RE/Hygro] Vector (Promega) using LipofectAMINE-2000, according to the manufacturer's protocol. pNL3.2.CMV Vector (Promega) was used as a negative control for experiments to measure regulated changes in NanoLuc® luciferase expression levels. After a total of 36 hr transfection, cells were trypsinized and seeded in 96-well plates at a density of 3 or 5×10^3 cells/well and cultured overnight in a complete EBM culture medium. Following day, cells were treated with TNF-α (20 ng/ml) or vehicle (PBS) for 5 hrs. Luciferase activity was measured using the Nano-Glo® Luciferase Assay System (Promega) with an EnSpire Multimode Plate Reader (PerkinElmer), and normalized to cell number. A representative of three independent experiments, each performed in sextuplicate, is depicted as mean fold induction vs. non-stimulated cells (PBS) (Gu et al., 2016; Seigner et al., 2019).

Adhesion assay

For quantitative assessment of T-cell adhesion to activated endothelium, we adapted previously published protocol (Wilhelmsen et al., 2013). Briefly, siRap1B or siControl-transfected HUVEC monolayers were treated with 50nM TNF-α (2% FBS EBM basal medium) for 12 hrs. Jurkat T cells were washed once with PBS and incubated in serum-free the RPMI-1640 medium with 5uM Calcein-AM (BD Biosciences-US) at 37 °C for 30 minutes. The stained Jurkat T cells were washed with PBS, and co-cultured with the TNF-α-treated HUVECs (1:1) for 45 min at 37 °C. Non-adherent Jurkat cells were removed by washing thrice with PBS. Calcein-AM fuorescence of EC-adhered Jurkat cells was immediately read on a fluorescence plate reader (Perkin Elmer EnSpire 2300) at 495/515 nm. Adhesion efficiency was calculated as a ratio of number of T cells bound per 10,000 cells plated.

Western blotting

For determination of CAM expression, siRap1B or siControl-transfected HUVECs were treated with 50nM TNF-α (2% FBS EBM basal medium) for 12 hrs. Following completion of adhesion assay, cells were lysed in RIPA cell lysis buffer (100mM Tris-HCl buffer (pH 7.4), 0.150M NaCl, 0.001M EDTA, 1% NP-40, 1% deoxycholic acid 0.1% SDS) with 2mM sodium orthovanadate and 1X protease/ phosphatase inhibitor cocktail. Cell lysates were clarified by centrifugation and protein concentration was determined PierceTMBCA protein assay kit (Thermo Scientific). Samples containing equal amount of protein were resolved on 4-12% gradient SDS-PAGE gels and transferred to PVDF membranes. PVDF membrane was blocked in 5% skim milk/(PBS and 0.05% Tween 20) for 1 hour at RT and probed with primary antibodies against VCAM-1 (Rabbit mAb #13662) and Rap1 (Rabbit mAb #2399), both Cell Signaling Technology), and β-actin (C4: sc-47778, Santa Cruz Biotechnology) overnight at 4^0C. Membranes were washed and incubated with horseradish peroxidase (HRP)-conjugated goat-anti-rabbit or donkey-anti mouse secondary antibodies for 1h at room temperature followed by chemiluminescence detection using ECL substrate (Pierce) and imaged using Amersham Imager 600 (GE Healthcare). Densitometric band intensity was determined using Amersham Imager 600 analysis software.

Statistical analysis

Sample sizes were calculated based on variability in our and others' previous studies. Animals were assigned to specific experimental groups without bias. When possible, subject randomization was achieved by distributing experimental groups across multiple cages and litters, as well as blinding during data collection and analysis to remove experimenter's bias. Graphs were generated and statistical analyses performed using GraphPad Prism version 9 (GraphPad Software). Graphs were represented as mean values and standard error of mean (S.E.M.). Student's t-test with Welch's correction was used to measure statistical significance between groups. For comparisons of more than two groups, one-way analysis of variance (ANOVA) with Tukey's multiple comparisons post hoc test was used. * $p<0.05$; ** $p<0.01$; *** $p<0.001$

Results

Endothelial Rap1B deletion blocks tumor growth and impairs tumor vascularization.

To assess the effect of Rap1B-deficiency on tumor growth we used B16F10 melanoma model. $Rap1B^{+/+}$ and $Rap1B^{+/-}$ mice were each injected with $2x10^5$ B16F10 melanoma cells and tumor

size was monitored until harvested for analysis on day 15 (Figure 1A). The tumor size was significantly smaller in Rap1B$^{+/-}$ mice, starting on day 8 after inoculation (Figure 1B, D). The final tumor weight was also decreased in Rap1B$^{+/-}$ mice compared to the wild-type control mice (Figure 1C). To determine the extent of endothelial Rap1B contribution to tumor growth, we examined melanoma growth in EC-specific Rap1B knockout (Rap1B$^{i\Delta EC}$) and Cdh5-Cre-negative control mice. Similar to total Rap1B depletion, endothelial deletion of Rap1B led to decreased tumor growth (Figure 1E) and decreased final weight and size of tumors (Figure 1F, G). Thus, these results suggest that the endothelial Rap1B significantly contributes to tumor growth.

Rap1B positively regulates developmental angiogenesis by promoting EC migration and proliferation (Carmona et al., 2009; Chrzanowska-Wodnicka et al., 2008). Thus, we next examined whether EC Rap1B-deficiency impaired tumor growth by decreasing neovascularization of tumors. Tumors were excised, digested with collagenase-dispase and endothelial compartment was quantitatively assessed in CD31 (PECAM-1)-positive and CD45-negative stained cells by flow cytometry (Figure 1 – figure supplement 1A, B). We found significantly decreased number of ECs/ per tumor weights in tumors from Rap1B$^{i\Delta EC}$ mice, compared to control mice (Figure 2A). A similar result was obtained in tumors from Rap1B$^{+/-}$ vs. control mice (Figure 1 – figure supplement 1C). Endothelial identity of the CD31-positive cells was further examined by immunohistochemistry in the tumor (Figure 1 – figure supplement 1D). Similar to the flow cytometry results, there was a significant decrease in CD31-positive cells in vascularized area in the tumor sections from Rap1B-deficient mice (Figure 1 – figure supplement 1E). These findings indicate that Rap1B-deficiency leads to impaired tumor endothelial cell endowment.

Endothelial Rap1B deletion leads to increased T-cell infiltration and adhesion to ECs.

Tumor ECs-driven angiogenesis supports tumor growth by providing blood flow to the ischemic tissue. Moreover, tumor ECs actively control leukocyte infiltration and activation states. To determine if the reduced tumor growth in Rap1B$^{i\Delta EC}$ mice is due to impaired angiogenesis or another aspect of endothelial function altered in the absence of Rap1B, we quantitatively characterized immunce cells from TME in control and Rap1B$^{i\Delta EC}$ mice. Single-cell suspensions from tumors from Rap1B$^{i\Delta EC}$ and control mice were stained with lymphoid and myeloid cell markers and examined by flow cytometry (Figure 2 – figure supplement 1A). Interestingly, we found that EC-Rap1B deficiency led to quantitative changes in the TME cellularity (Figure 2 – figure supplement 1B-F). Specifically, the number of infiltrated CD45^{+} leukocytes (Figure 2B),

and in particular, $CD4^+$ (Figure 2C) and $CD8^+$ (Figure 2D) T cells were increased in tumors from $Rap1B^{i\Delta EC}$ mice. To assess the effect of EC Rap1 deletion on CD45 activation, we examined surface expression of CD44, a cell-surface glycoprotein involved in cell-call interactions and a marker of T cell activation (Graham et al., 2007) in $Rap1B^{i\Delta EC}$ and control tumors. We found CD44 expression was significantly upregulated in $CD4^+$ (Figure 2E) and $CD8^+$ T-cells (Figure 2F) from $Rap1B^{i\Delta EC}$ mice. To further assess the level of T-cell activation, we examined intracellular expression of T-cell activation marker granzyme B (GrB) (Kelso et al., 2002). Consistently with increased T cell activation, we found increased number of GrB^+ $CD8^+$ T cells in tumors from $Rap1B^{i\Delta EC}$, vs. control mice (Figure 3G, H). Thus, EC-specific Rap1B knockout leads to decreased ECs in tumors, but increased leukocyte infiltration and increased leukocyte activity.

Depletion of $CD8^+$ T cells rescues tumor growth in $Rap1B^{i\Delta EC}$ mice

Increased presence of $CD8^+$ cytotoxic T cells is associated with reduced tumor growth (Ager et al., 2016; Joyce and Fearon, 2015). Our results showing increased leukocyte activation and recruitment to tumors in $Rap1B^{i\Delta EC}$ mice suggested endothelial Rap1B might control tumor growth by restricting $CD8^+$ T cell recruitment and activation. To determine if increased $CD8^+$-T-cell activity/infiltration was responsible for suppressed tumor growth in $Rap1B^{i\Delta EC}$ mice, we examined the effect of $CD8^+$ T-cell depletion *in vivo* on tumor growth and TME cellularity in $Rap1B^{i\Delta EC}$ and control mice (Figure 3A). Injection of anti-CD8α monoclonal antibody (mAb), successfully depleted $CD8^+$ T cells (Figure 3B), but not $CD4^+$ T cells (Figure 3 – figure supplement 1A) in tumors from control and $Rap1B^{i\Delta EC}$ mice. $CD8^+$ T cells were also depleted in other tissue compartments (blood, spleen and bone marrow, Figure 3 – figure supplement 2). Consistent with T-cell depletion, the overall number of $CD45^+$ cells was also decreased (Fig. 3F, Figure 3 – figure supplement 3). Interestingly, we found that the anti-CD8α Ab treatment did not lead to decreased tumor growth in control mice, compared to mice treated with isotype control mAb (Figure 3C). This further supports the view that in endothelial Rap1 restricts $CD8^+$ T cells' effector function and tissue homing in this aggressive melanoma mouse model. In contrast, anti-CD8α mAb injection restored tumor growth in $Rap1B^{i\Delta EC}$ mice to the level of control mice (Fig. 3C, Figure 3 – figure supplement 4).

We considered a possibility that restored tumor growth in $Rap1B^{i\Delta EC}$ mice upon depletion of $CD8^+$ T cell may be via increased angiogenesis (increased EC endowment) rather than altering of $CD8^+$ T cell -EC interactions. To this end, we examined EC endowment in tumors from control and $Rap1B^{i\Delta EC}$ mice (Figure 3D). Although $CD8^+$ T-cell depletion did not retard tumor

growth in normal mice, it resulted in a significant decrease in the number of tumor ECs, compared to isotype control mAb-injected mice (Figure 3E). This suggests that in control tumors, EC number is not a tumor growth-limiting factor. Interestingly, depletion of $CD8^+$ T cells lead to a small, but significant elevation of ECs numbers in tumors in $Rap1B^{i\Delta EC}$ mice (Figure 3E), albeit to a level lower than in WT IgG controls. These results show that restored tumor growth in $Rap1B^{i\Delta EC}$ mice is not likely due to improved angiogenesis, but rather inhibition of increased $CD8^+$ T cell activity upon deletion of Rap1B from endothelium.

Rap1B suppresses TNFα-induced NFκB transcription and signaling.

To gain insights into the mechanism through which Rap1B regulates the observed increased leukocyte recruitment and activity, we analyzed the global effects of the TME-associated cytokine, TNF-α treatment on gene expression in siRap1B and siControl ECs by bulk RNA sequencing. Principle component and differential gene expression analyses showed that siRap1B ECs exhibited a distinct transcriptional profile compared to siControl ECs (Figure 4 – figure supplement 1A, B). To assess the TNF-α-induced changes in ECs upon Rap1B knockdown, we conducted gene set enrichment analysis (GSEA) using gene sets from the Reactome database. This analysis revealed upregulation of genes in the TNF-α signaling pathway in siRap1B ECs (Figure 4A, B). Furthermore, the transcriptional profile was consistent with upregulation of NFκB transcriptional activity in siRap1B cells (Figure 4C, D and Figure 4 – figure supplement 1C, D). To examine the effect of Rap1B deletion on NFκB activity in ECs, siControl and siRap1B HUVECs were transfected with a NFκB-driven luciferase reporter plasmid or a control, empty plasmid, and emitted luminescence was measured after 5h cell exposure to TNF-α (20 ng/ml). TNF-α induced a modest, but significant luminescence increase in siControl ECs, vs. PBS (Figure 4E). Strikingly, TNF-α induced luminescence was significantly higher in siRap1B ECs (Figure 4E). Consistently with increased NFκB activity, GSEA revealed upregulation of NFκB targets (Figure 4F).

Notably, among NFκB-regulated genes upregulated in siRap1B ECs were proinflammatory Cell Adhesion Molecules (CAM)s; ICAM-1 and VCAM-1 (Figures 4B and F, asterisks). To validate these RNAseq data, we examined the effect of TNF-α on CAM protein expression in siRap1B and siControl ECs. TNF-α treatment led to a significant upregulation of VCAM-1 (Figure 5A) and ICAM-1 (Figure 5– figure supplement 1A) in control ECs. Interestingly, and consistent with increased transcript expression, TNF-α-induced CAM protein expression was significantly enhanced in Rap1B-deficient ECs (Figure 5A, Figure 5– figure supplement 1A). These findings show that in isolated ECs deletion of Rap1B leads to

upregulation of CAMs via upregulation of NFkB signaling in response to TME cytokine, TNF-α. Importantly, we found that, similarly to the *in vitro* effect, EC-Rap1B deletion mice led to elevated expression of VCAM (Figure 5B, C) and ICAM-1 (Figure 5– figure supplement 1B) in tumor ECs from Rap1B$^{i\Delta EC}$ vs. control mice. Thus, both *in vitro* and *in vivo*, EC Rap1B restricts CAM expression in response to a TME-associated cytokine.

EC-controlled expression of CAMs on EC surface controls leukocyte infiltration into tumors, by promoting leukocyte adhesion via integrins on leukocytes and CAMs on endothelium. To determine if increased adhesion to Rap1B-deficient endothelium may contribute to increased tumor infiltration, we measured the effect of TNF-α on leukocyte adhesion in Rap1B-deficient and WT ECs (Wilhelmsen et al., 2013) (Figure 5D). A 24-hour treatment with TNF-α led to a significant increase in leukocyte adhesion in control cells (Figure 5E). However, the number of leukocytes adhering to ECs was significantly increased upon Rap1B knockdown (Figure 5E), supporting our hypothesis that deletion of Rap1B in EC promotes EC-leukocyte interactions. In sum, underlying increased T-cell infiltration into Rap1B$^{i\Delta EC}$ tumors is elevated EC inflammatory NFkB activation and CAM expression, which leads to increased adhesion and activation of leukocytes.

Endothelial Rap1B mediates immune suppression in the VEGF pathway

In addition to stimulating EC angiogenic responses, VEGF promotes tumor growth by dampening EC responsiveness to proinflammatory cytokines and proinflammatory adhesion receptor expression, suppressing leukocyte recruitment. Because Rap1B is a positive regulator of VEGF-mediated angiogenic responses (Chrzanowska-Wodnicka, 2010; Lakshmikanthan et al., 2011), we hypothesized Rap1B may mediate VEGF-induced suppression of EC pro-inflammatory responses. To test this hypothesis, we examined the effect of Rap1B knockdown on VEGF-mediated modulation of VCAM-1 expression. Consistent with previous reports (Huang et al., 2015), TNF-α-induced VCAM-1 expression was largely inhibited in the presence of VEGF (Fig. 5F). Strikingly, this inhibitory effect of VEGF was abolished in siRap1B ECs, where VEGF failed to reduce TNF-α-induced VCAM-1 expression (Figure 5F). Therefore, Rap1B is an essential component of the VEGF signaling that modulates EC response to proinflammatory cytokines. Our findings suggest Rap1B may be a key EC signaling component mediating tumor EC anergy (vasosuppression).

Discussion

Overcoming vascular immunosuppression - reduced EC responsiveness to inflammatory stimuli - is essential for successful cancer immunotherapy. In this manuscript we demonstrate Rap1B is a key EC component restricting endothelial proinflammatory response. We show that EC Rap1B is permissive for tumor growth, as its EC deficiency suppresses tumor growth and angiogenesis. Perhaps more importantly, the deletion of Rap1B leads to altered TME, increased leukocyte recruitment, and, in particular, increased activity of tumor $CD8^+$ T cells. We find that tumor growth, albeit not angiogenesis, is restored in $Rap1B^{i\Delta EC}$ mice by depleting $CD8^+$ T cells. Therefore, the key function of Rap1B in tumor ECs is to control leukocyte, and specifically $CD8^+$ T cell interactions. Mechanistically, we show that Rap1B deletion leads to upregulation of the TNF-α signaling and cytokine-induced NFκB transcriptional activity. Specifically, EC Rap1B restricts proinflammatory cytokine-induced upregulation of CAMs on ECs and EC-leukocyte interactions *in vitro* and in tumor ECs, *in vivo*. Importantly, in the proangiogenic environment present in tumors, Rap1B is essential for mediating VEGF-immunosuppressive signaling, as Rap1-deficiency inhibits VEGF-mediated inhibition of CAM expression. Thus, our studies identify a novel EC-endogenous mechanism underlying VEGF-dependent desensitization of ECs to proinflammatory stimuli. Significantly, they identify EC Rap1B as a potential novel vascular adoptive cell therapy target.

Increased angiogenic factors in TME are linked with tumor progression and tumor vasculature has been a target of anti-tumor therapies (Ferrara and Adamis, 2016; Hendry et al., 2016). Anti-angiogenic therapies block vessel growth, normalize vascular permeability and promote the recruitment of pericytes to stabilize blood flow. Importantly, they sensitize anergic tumor endothelial cells to proinflammatory stimuli, induce proinflammatory expression program which promotes tumor-infiltrating T cells, a positive are prognostic for patient outcome in multiple cancers (Fridman et al., 2012). VEGF is the most prominent tumor angiogenic factor and a number of anti-VEGF therapies have been approved for treatment of cancer (Joyce and Fearon, 2015). However, anti-VEGF therapies lead to adverse effects (tumor aggressiveness, increased metastasis (Ebos et al., 2009; Pàez-Ribes et al., 2009). Moreover, while molecular pathways underlying VEGF-induced vessel formation have been intensely investigated, the mechanism through which VEGF modulates immune responses of tumor vessels remains poorly understood.

The findings described in this manuscript provide novel molecular insights into the molecular underpinnings of VEGF-induced immunosuppression. Previous studies implicated Rap1B

developmental angiogenesis (Chrzanowska-Wodnicka, 2013) and demonstrated that Rap1B controls multiple aspects of EC angiogenic responses to VEGF (Chrzanowska-Wodnicka, 2010). More recent, molecular studies demonstrated Rap1 acts as an upstream, positive regulator of VEGFR2 signaling important for shear stress sensing and NO release from ECs (Lakshmikanthan et al., 2015), and VEGF-induced vascular permeability (Lakshmikanthan et al., 2018). Consistently with that model, EC-Rap1B deficiency attenuates VEGF-induced permeability *in vivo* and protects from VEGF-induced hyperpermeability in a diabetes model (Lakshmikanthan et al., 2018). Here, we demonstrate, for the first time, to our knowledge, that Rap1 is essential for VEGF-induced inhibition of the proinflammatory response. While the exact molecular mechanisms need to be elucidated, our findings place Rap1B at the crossroads of VEGFR2 and cytokine signaling, essential for control of tumor growth (Fig. 6).

An unbiased transcriptomics approach provided a novel, global view of pathways controlled by Rap1B (Figure 4 and Figure 4 – figure supplement 1). The top pathway upregulated in the absence of Rap1B is the NFκB -mediated proinflammatory response. Deletion of Rap1B leads to upregulation of NFκB targets, including CAM receptors, both: *in vitro* and in tumor ECs *in vivo*. Interestingly, Rap1B deletion also leads to upregulation of CAMs in a mouse atherosclerosis model (Singh et al., 2021). Additional NFκB proinflammatory targets likely contribute to the increased leukocyte infiltration and leukocyte infiltration in Rap1B$^{i\Delta EC}$ tumors, and warrant further investigation. The analysis of Rap1B$^{i\Delta EC}$ TME cellularity revealed that EC Rap1B-deficiency selectively affected other leukocyte populations; in particular the number of some tumor B cells was increased in Rap1B$^{i\Delta EC}$ tumors vs. controls (Figure 2 - figure supplement 1D, E). Future studies will determine whether these effects are primary or secondary. Nonetheless, our findings support Rap1B as a key regulator of EC-leukocyte interactions via a novel mechanism involving suppression of proinflammatory signaling. These results also reveal a new aspect of Rap1 biology in endothelium. Future studies will focus on the mechanisms of transcriptional control by Rap1B and their implications in proinflammatory states.

In sum, we identified Rap1B as a novel molecular regulator of EC proinflammatory response, which may lead to new therapeutic approaches to overcome vascular immunosuppression in cancer immunotherapy.

Figure, figure supplements and figure source data legends

Figure 1. Global and EC-specific Rap1B deletion restricts tumor growth in vivo.

(A) A schematic diagram of melanoma induction in global Rap1B-deficient mice, $Rap1B^{+/-}$, or EC-specific Rap1B knockouts, $Rap1B^{i\Delta EC}$. Tumor growth kinetics **(B),** tumor weight at day 15 **(C)** and representative photographs of melanoma growth **(D)** in $Rap1B^{+/-}$ (n=10) vs. $Rap1B^{+/+}$ (n=10) mice. Tumor growth kinetics **(E)**, tumor weights **(F)** and representative photographs of melanoma growth **(G)** in $Rap1B^{i\Delta EC}$ (n=5) vs. Cre-negative control mice (n=6). Data represent mean ± SEM. *, P < 0.05 **, P < 0.01, ***, P < 0.001, Student's *t* test. Data and statistical outputs are available in *Figure 1-source data 1* file.

Figure 1-source data 1*:* relates to panels A-F.

Figure 1- figure supplement 1. Reduced $CD31^+$ endothelial cells in $Rap1B^{+/-}$ tumors. (**A**). Gating strategy for endothelial cells ($CD31^+$) and leukocytes ($CD45^+$) using stained single-cell suspension from the harvested tumors. Representative plots from a control tumor are shown. One million events were acquired on BD FACS-diva (LSR II-Green) using single-cell suspension from the harvested tumors. Viable, 7-AAD-negative cells were identified, and cell doublets were discriminated by their SSC and FSC characteristics. Single cells were further gated for leukocytes ($CD45^+/CD31^-$) and endothelial cells ($CD31^+/CD45^-$). (**B**) Decreased number of tumor endothelial cells ($CD31^+/CD45^-$) isolated from $Rap1B^{+/-}$ mice vs. control, shown as % of gated single cells (**C** *, P < 0.05). Data are presented as the mean ± S.E.M. n = 5 mice per group, student's *t* test. (**D**) Typical immunofluorescent staining of $CD45^+$ cells (green) and $CD31^+$ endothelial cells (red) in tumor sections. (**E**) $CD31^+$ endothelial cells quantification demonstrates a significant decrease in ECs in tumor sections in $Rap1B^{+/-}$, vs. control group (*, P < 0.05). n = 3 mice per group, Student's *t* test. Data and statistical outputs are available in *Figure 1 – figure supplement 1-source data 1* file.

Figure 1 – figure supplement 1-source data 1: relates to panels C and E.

Figure 2. Endothelial Rap1B restricts tumor T-cell infiltration. (A-D) Endothelial Rap1B-deficiency alters TME cellularity. Flow cytometry analysis of single cell suspensions from tumors stained with cell-type specific markers demonstrate decreased endothelial cell numbers ($CD31^+$, **A),** and increased $CD45^+$ cells **(B)** in $Rap1B^{i\Delta EC}$ (n=5) vs. control mice (n=5). Gating strategy shown in Supplementary Fig. S1. $CD4^+$ T cells **(C)** and $CD8^+$ T cells **(D)** selected as shown in gating scheme in Supplementary Figure S3. (**E-H**) **Elevated T cell activation in $Rap1B^{i\Delta EC}$ vs. control mice.** Surface expression of T-cell activation marker CD44 in $CD4^+$T **(E)** and $CD8^+$T **(F)** cells in $Rap1B^{i\Delta EC}$ (n=5) and control mice (n=6) tumors. **(G-H)** Representative

FACS plots (**G**) and quantification of median fluorescence intensity, (MFI, **H**) of intracellular staining for granzyme B (GrB) in tumor CD8$^+$ T cells from Rap1B$^{i\Delta EC}$ (n=8) and control mice (n=5). Data represent mean ± SEM. *, P < 0.05 **, P < 0.01, ***, P < 0.001, Student's t-test. Data and statistical outputs are available in *Figure 2-source data 1* file.

Figure 2-source data 1: relates to panels A-F, H.

Figure 2-figure supplement 1. EC-specific Rap1B deletion alters recruitment of tumor-infiltrating lymphocytes (TIL). (**A**) Gating and selection of immune cell types from tumor single-cell suspensions. Representative plots from a control tumor are shown. One million events were acquired on BD FACS-diva (LSR II-Green) using single-cell suspension from the harvested tumors. Single cells were used to identify CD45$^+$ leukocytes, which were further gated using marker-specific antibodies against NK1.1 (natural killer cells), CD4, CD8 and B220 B-cells. **B-F.** Quantitation of cell populations: **(B)** B cells (B220$^+$), **(C)** natural killer cells (NK1.1$^+$), **(D)** myeloid cells (CD11b$^+$), **(E)** monocytes (Ly6C$^+$) and **(F)** macrophage (F4/80$^+$) in single-cell suspension of tumors from Rap1B$^{i\Delta EC}$ or control mice. Data are presented as the mean ± S.E.M. *, P < 0.05. n = 5 mice per group, Student's *t* test. Data and statistical outputs are available in *Figure 2– figure supplement 1-source data 1* file.

Figure 2– figure supplement 1-source data 1: relates to panels B-F.

Figure 3. Depletion of CD8$^+$ T cells normalizes tumor growth in Rap1B$^{i\Delta EC}$ mice.

(A) Schematic diagram of antibody treatment (intraperitoneal, I.P. injection) and melanoma induction (subcutaneous, S.C. injection). **(B)** Quantification of CD8$^+$ T cells demonstrates highly efficient cell depletion in with anti-CD8 antibody or IgG isotype control. **(C)** Tumor growth kinetics in Rap1B$^{i\Delta EC}$ vs. Cre-negative control treated with anti-CD8 . **(D)** Gating scheme and quantification of CD31$^+$ ECs **(E)** and CD45$^+$ cells **(F).** Data are presented as the mean ± S.E.M (n=6 per group). *, P < 0.05, **, P < 0.01, ***, P < 0.001, Panels B, C, F: one-way ANOVA with Tukey's post hoc test. Panel E: Student's t-test. Data and statistical outputs are available in *Figure 3-source data 1* file.

Figure 3-source data 1: relates to panels B, C, E and F.

Figure 3 – figure supplement 1. Efficiency of CD8$^+$ T cell depletion in specific tissue compartments.

Peripheral blood cells **(A)**, spleen cells **(B)** and bone marrow cells (**C)** were stained with Very CD8 mAb. Flow analysis showing drastic depletion of CD8$^+$ cells in all tissue compartment. IgG isotype control has no significant modulation on T cell. Data are presented as the mean ± S.E.M. ***, P < 0.001, ****, P < 0.0001. n = 6 mice per group, one-way ANOVA with Tukey's

multiple comparisons post hoc test. Data and statistical outputs are available in *Figure 3 – figure supplement 1-source data 1* file.

Figure 3 – figure supplement 1-source data 1: relates to panels A-F.

Figure 3 – figure supplement 2. Hematological (CBC) analysis in control and Rap1B$^{i\Delta EC}$ mice after CD8^{+} T cell depletion. Whole blood (13 µl per mouse) was collected into anticoagulant (1:10) using capillary tubes (StatSpin® Microhematocrit Tubes, VWR). The blood samples were immediately analyzed using an automated Hematology blood analyzer (Sysmex XN-1000™). CBC counts: **(A)** White blood cells (WBC) 10^9/L; **(B)** lymphocyte (LYMPH) 10^9/L. **(C)** Immature (young) RBC fraction, as measured by % of high fluorescence reticulocyte (HFR), **(D)** Platelets (PLT) 10^{12}/L, **(E)** Red blood cells (RBC) 10^{12}/L, and **(F)** Neutrophils (NEUT). Data are presented as the mean ± S.E.M. *, $P < 0.05$, **, $P < 0.01$. n = 6 mice per group, one-way ANOVA with Tukey's multiple comparisons post hoc test. Data and statistical outputs are available in *Figure 3 – figure supplement 2-source data 1* file.

Figure 3 – figure supplement 2-source data 1: relates to panels A-C.

Figure 3 – figure supplement 3. Effect of CD8^{+} T-cell depletion on tumor-infiltrating lymphocytes (TIL) in control and Rap1B$^{i\Delta EC}$ mice. Immunophenotypic examination showing quantitation of **(A)** CD4^{+}T cells, **(B)** B cells (B220^{+}), **(C)** myeloid cells (CD11b^{+}), **(D)** monocytes (Ly6C^{+}), **(E)** neutrophils (Ly6G^{+}) and **(F)** macrophage (F4/80^{+}) in Rap1B$^{i\Delta EC}$/control mice treated with either IgG isotope or CD8 mAb. Data are presented as the mean ± S.E.M. *, $P < 0.05$, **, $P < 0.01$. n = 6 mice per group, one-way ANOVA with Tukey's multiple comparisons post hoc test. Data and statistical outputs are available in *Figure 3 – figure supplement 3-source data 1* file.

Figure 3 – figure supplement 3-source data 1: relates to panels A-F.

Figure 3 – figure supplement 4. Depletion of CD8^{+} T-cells normalizes tumor growth in Rap1B$^{i\Delta EC}$ mice. Representative photographs showing pattern of tumor growth in Rap1B$^{i\Delta EC}$/control mice treated with either IgG isotope or CD8 mAb. **(A)** IgG isotope has no effect on tumor growth in control group. **(B)** CD8^{+} T cell depletion significantly rescued tumor reduction in Rap1B$^{i\Delta EC}$ mice group.

Figure 4. Endothelial Rap1B restricts TNF-α induced NFκB activation.

Increased TNF-α signaling and NFκB transcription detected by bulk RNA sequencing of TNF-α-treated siRap1B and siControl Ecs. **(A)** Gene set enrichment analysis (GSEA) of genes in TNF-α signaling pathway upregulated in siRap1B vs. siControl. **(B)** Heatmap of selected genes from TNF-α signaling pathway. **(C)** GSEA of NFκB signaling pathway. **(D)** Transcriptional activation of NFκB in siRap1B ECs. **(E)** TNF-α-induced NFκB activity determined by luciferase assay in

cells transfected with NF-κB reporter construct or a control vector (CMV). Values shown as mean fold change vs. PBS-treated cells . Error bars represent mean ± SD (n = 6). *, P < 0.05, ****, P < 0.0005. One-way ANOVA followed by Tukey's multiple comparisons test. **(F)** Heatmap of selected genes from NFκB pathway. (n = 5 separate EC sets per group). Link to sequence data deposited within NCBI GEO is available in *Figure 4-source data 1* file. Data and statistical outputs for panel E are available in *Figure 4-source data 2* file.

Figure 4-source data 1: relates to panels A-D and F.

Figure 4-source data 2: relates to panel E.

Figure 4 – figure supplement 1. Transcriptomic analysis of TNF-α-stimulated siControl and siRap1B ECs. (A) Principal component analysis of samples. (**B**) Volcano plot of differential gene expression, the top 50 significantly differentially expressed genes are labeled. (**C**) Gene set enrichment analyses (GSEA) of NFκB target genes. (**D**) Dot plot of top significantly enriched transcription factors by GSEA (n = 5). Link to sequence data deposited within NCBI GEO is available in *Figure 4-source data 1* file.

Figure 5. Endothelial Rap1B restricts proinflammatory CAM expression, mediates VEGF signaling. (A) Top: Densitometry of TNFα-induced VCAM-1 expression, normalized to actin, in siControl- or siRap1B- transfected HUVECs. Bottom: representative Western blot. Original images are available in *Figure 5-source data 1* file. **(B, C)** VCAM-1 expression in tumor ECs ($CD31^+$ cells): representative flow cytometry histogram (**B**) and median fluorescence intensity (MFI) (**C**). n ≥ 5 mice per group, **(D, E)** EC-Rap1B deficiency leads to increased leukocyte adhesion in vitro. Representative image (**D**) and quantification (**E**) of Calcein-AM-labeled Jurkat cells adhering to siRap1B and siControl ECs following TNF-α treatment 12 hours. Adhesion efficiency is expressed as Jurkat cells bound/10,000 plated. (**F**) VEGF treatment inhibits TNF-α-induced CAM expression in siControl but not in siRap1B ECs. Densitometry (top) and representative Western blot (bottom) are shown. Original images are available in *Figure 5-source data 2* file. Data shown are mean ± S.E.M. *, P < 0.05, **, P < 0.01, ***, P < 0.001, Panels A, E, F: one-way ANOVA followed by Tukey's multiple comparisons test. Panel C: Student's t-test. Data and statistical outputs are available in *Figure 5-source data 3* file.

Figure 5-source data 1: original images of Western blots in panel A.

Figure 5-source data 2: original images of Western blots in panel F.

Figure 5-source data 3: relates to panels A, C, E and F.

Figure 5 – figure supplement 1. Elevated ICAM-1 surface expression in Rap1B-deficient tumor ECs and HUVECs. (A) Flow cytometric analysis of ICAM-1 expression on siRap1B and

siControl HUVEC cells. (**B**) Flow cytometric analysis of ICAM-1 expression on tumor ECs from Rap1B$^{i\Delta EC}$ and control mice**:** representative flow cytometry histogram and median fluorescence intensity (MFI) plot (**C**). Data are presented as the mean ± S.E.M. **, P < 0.01, Student's t test. Data and statistical outputs are available in *Figure 5 – figure supplement 1-source data 1* file.

Figure 5 – figure supplement 1-source data 1: relates to panels A and C.

Figure 6. Endothelial Rap1B conveys VEGF suppression of immune reactivity – proposed mechanism. Under normal conditions Rap1 suppresses cytokine-induced CAM expression, limiting T-cell adhesion and recruitment. In proangiogenic conditions of TME, VEGF signaling, mediated by Rap1B, suppresses this endothelial immune response.

References

Ager, A., H.A. Watson, S.C. Wehenkel, and R.N. Mohammed. 2016. Homing to solid cancers: A vascular checkpoint in adoptive cell therapy using CAR T-cells. *Biochemical Society Transactions*. 44:377-385.

Benjamini, Y., and Y. Hochberg. 1995. Controlling the False Discovery Rate: A Practical and Powerful Approach to Multiple Testing. *Journal of the Royal Statistical Society. Series B (Methodological)*. 57:289-300.

Boettner, B., and L. Van Aelst. 2009. Control of cell adhesion dynamics by Rap1 signaling. *Current Opinion in Cell Biology*. 21:684-693.

Carmona, G., S. Gottig, A. Orlandi, J. Scheele, T. Bauerle, M. Jugold, F. Kiessling, R. Henschler, A.M. Zeiher, S. Dimmeler, and E. Chavakis. 2009. Role of the small GTPase Rap1 for integrin activity regulation in endothelial cells and angiogenesis. *Blood*. 113:488-497.

Chrzanowska-Wodnicka, M. 2010. Regulation of angiogenesis by a small GTPase Rap1. *Vascular Pharmacology*. 53:1-10.

Chrzanowska-Wodnicka, M. 2013. Distinct functions for Rap1 signaling in vascular morphogenesis and dysfunction. *Experimental Cell Research*. 319:2350-2359.

Chrzanowska-Wodnicka, M., A.E. Kraus, D. Gale, G.C. White, 2nd, and J. Vansluys. 2008. Defective angiogenesis, endothelial migration, proliferation, and MAPK signaling in Rap1b-deficient mice. *Blood*. 111:2647-2656.

Chrzanowska-Wodnicka, M., S.S. Smyth, S.M. Schoenwaelder, T.H. Fischer, and G.C. White. 2005. Rap1b is required for normal platelet function and hemostasis in mice. *Journal of Clinical Investigation*. 115:2296-2296.

Dirkx, A.E.M., M.G.A. Oude Egbrink, K. Castermans, D.W.J. Van Der Schaft, V.L.J.L. Thijssen, R.P.M. Dings, L. Kwee, K.H. Mayo, J. Wagstaff, J.C.A. Bouma-ter Steege, and A.W. Griffioen. 2006. Anti-angiogenesis therapy can overcome endothelial cell anergy and promote leukocyte-endothelium interactions and infiltration in tumors. *FASEB Journal*. 20:621-630.

Ebos, J.M.L., C.R. Lee, W. Cruz-Munoz, G.A. Bjarnason, J.G. Christensen, and R.S. Kerbel. 2009. Accelerated Metastasis after Short-Term Treatment with a Potent Inhibitor of Tumor Angiogenesis. *Cancer Cell*. 15:232-239.

Fabregat, A., S. Jupe, L. Matthews, K. Sidiropoulos, M. Gillespie, P. Garapati, R. Haw, B. Jassal, F. Korninger, B. May, M. Milacic, C.D. Roca, K. Rothfels, C. Sevilla, V. Shamovsky, S. Shorser, T. Varusai, G. Viteri, J. Weiser, G. Wu, L. Stein, H. Hermjakob,

and P. D'Eustachio. 2018. The Reactome Pathway Knowledgebase. *Nucleic Acids Research*. 46:D649-D655.

Ferrara, N., and A.P. Adamis. 2016. Ten years of anti-vascular endothelial growth factor therapy. *Nature Reviews Drug Discovery*. 15:385-403.

Fridman, W.H., F. Pagès, C. Sautès-Fridman, and J. Galon. 2012. The immune contexture in human tumours: Impact on clinical outcome. *Nature Reviews Cancer*. 12:298-306.

Graham, V.A., A.L. Marzo, and D.F. Tough. 2007. A role for CD44 in T cell development and function during direct competition between CD44+ and CD44– cells. *European Journal of Immunology*. 37:925-934.

Griffioen, A.W., C.A. Damen, S. Martinotti, G.H. Blijham, and G. Groenewegen. 1996. Endothelial intercellular adhesion molecule-1 expression is suppressed in human malignancies: The role of angiogenic factors. *Cancer Research*. 56:1111-1117.

Gu, S.X., I.O. Blokhin, K.M. Wilson, N. Dhanesha, P. Doddapattar, I.M. Grumbach, A.K. Chauhan, and S.R. Lentz. 2016. Protein methionine oxidation augments reperfusion injury in acute ischemic stroke. *JCI insight*. 1.

Hendry, S.A., R.H. Farnsworth, B. Solomon, M.G. Achen, S.A. Stacker, and S.B. Fox. 2016. The role of the tumor vasculature in the host immune response: Implications for therapeutic strategies targeting the tumor microenvironment. *Frontiers in Immunology*. 7.

Huang, H., E. Langenkamp, M. Georganaki, A. Loskog, P.F. Fuchs, L.C. Dieterich, J. Kreuger, and A. Dimberg. 2015. VEGF suppresses T-lymphocyte infiltration in the tumor microenvironment through inhibition of NF-κB-induced endothelial activation. *FASEB Journal*. 29:227-238.

Joyce, J.A., and D.T. Fearon. 2015. T cell exclusion, immune privilege, and the tumor microenvironment. *Science*. 348:74-80.

Kelso, A., E.O. Costelloe, B.J. Johnson, P. Groves, K. Buttigieg, and D.R. Fitzpatrick. 2002. The genes for perforin, granzymes A–C and IFN-γ are differentially expressed in single CD8+ T cells during primary activation. *International Immunology*. 14:605-613.

Lakshmikanthan, S., M. Sobczak, C. Chun, A. Henschel, J. Dargatz, R. Ramchandran, and M. Chrzanowska-Wodnicka. 2011. Rap1 promotes VEGFR2 activation and angiogenesis by a mechanism involving integrin alphavbeta(3). *Blood*. 118:2015-2026.

Lakshmikanthan, S., M. Sobczak, S. Li Calzi, L. Shaw, M.B. Grant, and M. Chrzanowska-Wodnicka. 2018. Rap1B promotes VEGF-induced endothelial permeability and is required for dynamic regulation of the endothelial barrier. *Journal of Cell Science*. 131.

691 Lakshmikanthan, S., X. Zheng, Y. Nishijima, M. Sobczak, A. Szabo, J. Vasquez-Vivar, D.X.
692 Zhang, and M. Chrzanowska-Wodnicka. 2015. Rap1 promotes endothelial
693 mechanosensing complex formation, NO release and normal endothelial function.
694 *EMBO Reports*. 16:628-637.
695 Ley, K., C. Laudanna, M.I. Cybulsky, and S. Nourshargh. 2007. Getting to the site of
696 inflammation: The leukocyte adhesion cascade updated. *Nat. Rev. Immunol.* 7:678-689.
697 Liberzon, A., A. Subramanian, R. Pinchback, H. Thorvaldsdóttir, P. Tamayo, and J.P. Mesirov.
698 2011. Molecular signatures database (MSigDB) 3.0. *Bioinformatics*. 27:1739-1740.
699 Love, M.I., W. Huber, and S. Anders. 2014. Moderated estimation of fold change and dispersion
700 for RNA-seq data with DESeq2. *Genome Biology*. 15.
701 Ogata, H., S. Goto, K. Sato, W. Fujibuchi, H. Bono, and M. Kanehisa. 1999. KEGG: Kyoto
702 encyclopedia of genes and genomes. *Nucleic Acids Research*. 27:29-34.
703 Pàez-Ribes, M., E. Allen, J. Hudock, T. Takeda, H. Okuyama, F. Viñals, M. Inoue, G. Bergers,
704 D. Hanahan, and O. Casanovas. 2009. Antiangiogenic Therapy Elicits Malignant
705 Progression of Tumors to Increased Local Invasion and Distant Metastasis. *Cancer Cell*.
706 15:220-231.
707 Patro, R., G. Duggal, M.I. Love, R.A. Irizarry, and C. Kingsford. 2017. Salmon provides fast and
708 bias-aware quantification of transcript expression. *Nature Methods*. 14:417-419.
709 Piali, L., A. Fichtd, H.J. Terpe, B.A. Imhof, and R.H. Gisler. 1995. Endothelial vascular cell
710 adhesion molecule 1 expression is suppressed by melanoma and carcinoma. *Journal of*
711 *Experimental Medicine*. 181:811-816.
712 Picelli, S., O.R. Faridani, Å.K. Björklund, G. Winberg, S. Sagasser, and R. Sandberg. 2014. Full-
713 length RNA-seq from single cells using Smart-seq2. *Nat. Protoc.* 9:171-181.
714 Seigner, J., M. Junker-Samek, A. Plaza, G. D'Urso, M. Masullo, S. Piacente, Y.M. Holper-
715 Schichl, and R. de Martin. 2019. A Symphytum officinale Root Extract Exerts Anti-
716 inflammatory Properties by Affecting Two Distinct Steps of NF-κB Signaling. *Front*
717 *Pharmacol*. 10:289-289.
718 Shrimali, R.K., Z. Yu, M.R. Theoret, D. Chinnasamy, N.P. Restifo, and S.A. Rosenberg. 2010.
719 Antiangiogenic agents can increase lymphocyte infiltration into tumor and enhance the
720 effectiveness of adoptive immunotherapy of cancer. *Cancer Research*. 70:6171-6180.
721 Singh, B., R. Kosuru, S. Lakshmikanthan, M.G. Sorci-Thomas, D.X. Zhang, R. Sparapani, J.
722 Vasquez-Vivar, and M. Chrzanowska. 2021. Endothelial Rap1 (Ras-Association
723 Proximate 1) Restricts Inflammatory Signaling to Protect From the Progression of
724 Atherosclerosis. *Arteriosclerosis, Thrombosis, and Vascular Biology*. 41:638-650.

Subramanian, A., P. Tamayo, V.K. Mootha, S. Mukherjee, B.L. Ebert, M.A. Gillette, A. Paulovich, S.L. Pomeroy, T.R. Golub, E.S. Lander, and J.P. Mesirov. 2005. Gene set enrichment analysis: A knowledge-based approach for interpreting genome-wide expression profiles. *Proceedings of the National Academy of Sciences of the United States of America*. 102:15545-15550.

Wilhelmsen, K., K. Farrar, and J. Hellman. 2013. Quantitative in vitro assay to measure neutrophil adhesion to activated primary human microvascular endothelial cells under static conditions. *Journal of visualized experiments : JoVE*:e50677-e50677.

Xin, G., A. Khatun, P. Topchyan, R. Zander, P.J. Volberding, Y. Chen, J. Shen, C. Fu, A. Jiang, W.A. See, and W. Cui. 2020. Pathogen-boosted adoptive cell transfer therapy induces endogenous antitumor immunity through antigen spreading. *Cancer Immunology Research*. 8:7-18.

Yan, J., F. Li, D.A. Ingram, and L.A. Quilliam. 2008. Rap1a is a key regulator of fibroblast growth factor 2-induced angiogenesis and together with Rap1b controls human endothelial cell functions. *Molecular and Cellular Biology*. 28:5803-5810.

Supplemental Table 1: Key Resources and Antibodies

Reagent type (species) or resource	Designation	Source or reference	Identifiers	Additional information
(Mus musculus)	VE-Cadh-CreN-Rap1a$^{+/+}$Rap1b$^{f/f}$	In house breeding		C57Bl/6 genetic background
(Mus musculus)	VE-Cadh-CreY-Rap1a$^{+/+}$Rap1b$^{f/f}$	In house breeding		C57Bl/6 genetic background
(Mus musculus)	Rap1B$^{(+/-)}$	In house breeding		C57Bl/6 genetic background
(Mus musculus)	Rap1B$^{(+/+)}$	In house breeding		C57Bl/6 genetic background
Other	HUVECs(Human Umbilical Vein ECs)	ATCC	Cat# CRL-1730 RRID:CVCL_2959	
Other	B16F10	ATCC	Cat# CRL-6475 RRID:CVCL_0159	Mouse melanoma cell line
Other	Jurkat E6–1	ATCC	Cat# TIB-152	Human T cell leukemia cell line
Other	Rap1B siRNA	Dharmacon		50nM in reaction
Other	Control siRNA	Dharmacon		50nM in reaction
Chemical compound, drug	TNF-α	Sigma-Aldrich	Cat# H8916-10UG	50nM in assay
Chemical compound, drug	VEGF	Sigma-Aldrich	Cat# V7259	50 ng/ml in assay
Chemical compound, drug	Calcein Blue AM	BD Biosciences	Cat# 564060	5uM in assay
Other	pNL3.2.NF-κB-RE[NlucP/NF-κB-RE/Hygro] Vector	Promega	Cat#N1111	2 ug in assay
Other	pNL3.2.CMV	Promega	Cat#N1411	2 ug in assay
Assay kit	Nano-Glo® Luciferase Assay System	Promega	Cat.# N1110	
Antibody	VCAM-1 (clone E1E8X) Rabbit mAb antibody	Cell Signaling Technology	Cat# 13662, RRID:AB_2798286	WB (1:2000)
Antibody	Rap1A/Rap1B (clone 26B4) Rabbit mAb antibody	Cell Signaling Technology	Cat# 2399, RRID:AB_2284915	WB (1:2000)
Antibody	β-Actin mouse, rat, human (clone C4) mAb antibody	Santa Cruz Biotechnology	Cat# sc-47778 RRID:AB_2714189	WB (1:500)
Software, algorithm	GraphPad Prism version 5.02	GraphPad Software		
Software, algorithm	Flow Jo software			
Antibody	FITC anti-mouse CD3, clone: 145-2C11	Bio Legend	Cat# 100305, RRID:AB_312670	Dilution: 1:300 For Tumor Infiltrate Lymphocyte (TIL)

	(Armenian Hamster-monoclonal)			analysis by flow cytometry
Antibody	APC anti-mouse CD4, Clone GK1.5, (rat-monoclonal)	Bio Legend	Cat# 100412, RRID:AB_312697	Dilution: 1:400 For TIL analysis by flow cytometry
Antibody	FITC anti-mouse CD4, Clone GK1.5, (rat-monoclonal)	Bio Legend	Cat# 100405, RRID:AB_312690	Dilution: 1:400 For TIL analysis by flow cytometry
Antibody	Brilliant Violet 510(TM) anti-mouse, Clone M1/70, (rat-monoclonal)	Bio Legend	Cat# 101263, RRID:AB_2629529	Dilution: 1:400 For TIL analysis by flow cytometry
Antibody	PE/Cyanine7 anti-mouse CD31, Clone 390, (rat-monoclonal)	Bio Legend	Cat# 102418, RRID:AB_830757	Dilution: 1:300 For TIL analysis by flow cytometry
Antibody	APC/Cyanine7 anti-mouse CD44, Clone IM7, (rat-monoclonal)	Bio Legend	Cat# 103028, RRID:AB_830785	Dilution: 1:400 For TIL analysis by flow cytometry
Antibody	PE/Cyanine5 anti-mouse CD45, Clone 30-F11, (rat-monoclonal)	Bio Legend	Cat# 103109, RRID:AB_312974	Dilution: 1:400 For TIL analysis by flow cytometry
Antibody	APC/Cyanine7 anti-mouse CD45, Clone 30-F11, (rat-monoclonal)	Bio Legend	Cat# 103116, RRID:AB_312981	Dilution: 1:400 For TIL analysis by flow cytometry
Antibody	PE/Dazzle(TM) 594 anti-mouse, clone RA3-6B2, (rat-monoclonal)	Bio Legend	Cat# 103258, RRID:AB_2564053	Dilution: 1:200 For TIL analysis by flow cytometry
Antibody	Pacific Blue(TM) anti-mouse F4/80, Clone BM8, (rat-monoclonal)	Bio Legend	Cat# 123124, RRID:AB_893475	Dilution: 1:300 For TIL analysis by flow cytometry
Antibody	Alexa Fluor(R) 700 anti-mouse Ly-6G, Clone 1A8, (rat-monoclonal)	Bio Legend	Cat# 127622, RRID:AB_10643269	Dilution: 1:300 For TIL analysis by flow cytometry
Antibody	PE anti-mouse Ly-6C, Clone HK1.4, (rat-monoclonal)	Bio Legend	Cat# 128007, RRID:AB_1186133	Dilution: 1:300 For TIL analysis by flow cytometry
Antibody	PerCP anti-mouse Ly-6G/Ly-6C (Gr-1), Clone RB6-8C5, (rat-monoclonal)	Bio Legend	Cat# 108425, RRID:AB_893560	Dilution: 1:400 For TIL analysis by flow cytometry
Antibody	APC anti-mouse NK-1.1, Clone PK136, (rat-	Bio Legend	Cat# 108709, RRID:AB_313396	Dilution: 1:200 For TIL analysis by flow cytometry

	monoclonal)			
Antibody	PE anti-mouse CD8a, Clone 53-6.7, (rat-monoclonal)	Thermo Fisher Scientific	Cat# 12-0081-82, RRID:AB_465530	Dilution: 1:200 For TIL analysis by flow cytometry
Antibody	eFluor 450 anti-mouse CD106 (VCAM-1), Clone 429, (rat-monoclonal)	Thermo Fisher Scientific	Cat# 48-1061-82, RRID:AB_1633378)	Dilution: 1:300 For TIL analysis by flow cytometry
Antibody	FITC anti-mouse CD54 (ICAM-1), Clone YN1/1.7.4, (rat-monoclonal)	Thermo Fisher Scientific	Cat# 11-0541-82, RRID:AB_465094)	Dilution: 1:300 For TIL analysis by flow cytometry
Antibody	PE cy7 anti-mouse Granzyme B, Clone NGZB, (rat-monoclonal)	Thermo Fisher Scientific	Cat# 25-8898-82, RRID:AB_10853339	Dilution: 1:200 For TIL analysis by flow cytometry
Antibody	eFluor 450-Rat IgG1 κ Isotype control, Clone eBRG1, (rat-monoclonal)	Thermo Fisher Scientific	Cat# 48-4301-82, RRID:AB_1271984	Dilution: 1:200 For FMO control in flow cytometry
Antibody	PE cy7-Rat IgG2a κ Isotype control, Clone eBR2a, (rat-monoclonal)	Thermo Fisher Scientific	Cat# 25-4321-82, RRID:AB_470200	Dilution: 1:200 For FMO control in flow cytometry
Antibody	FITC-Rat IgG2b κ Isotype control, Clone eB149/10H5, (rat-monoclonal)	Thermo Fisher Scientific	Cat# 11-4031-82, RRID:AB_470004)	Dilution: 1:200 For FMO control in flow cytometry

744
745

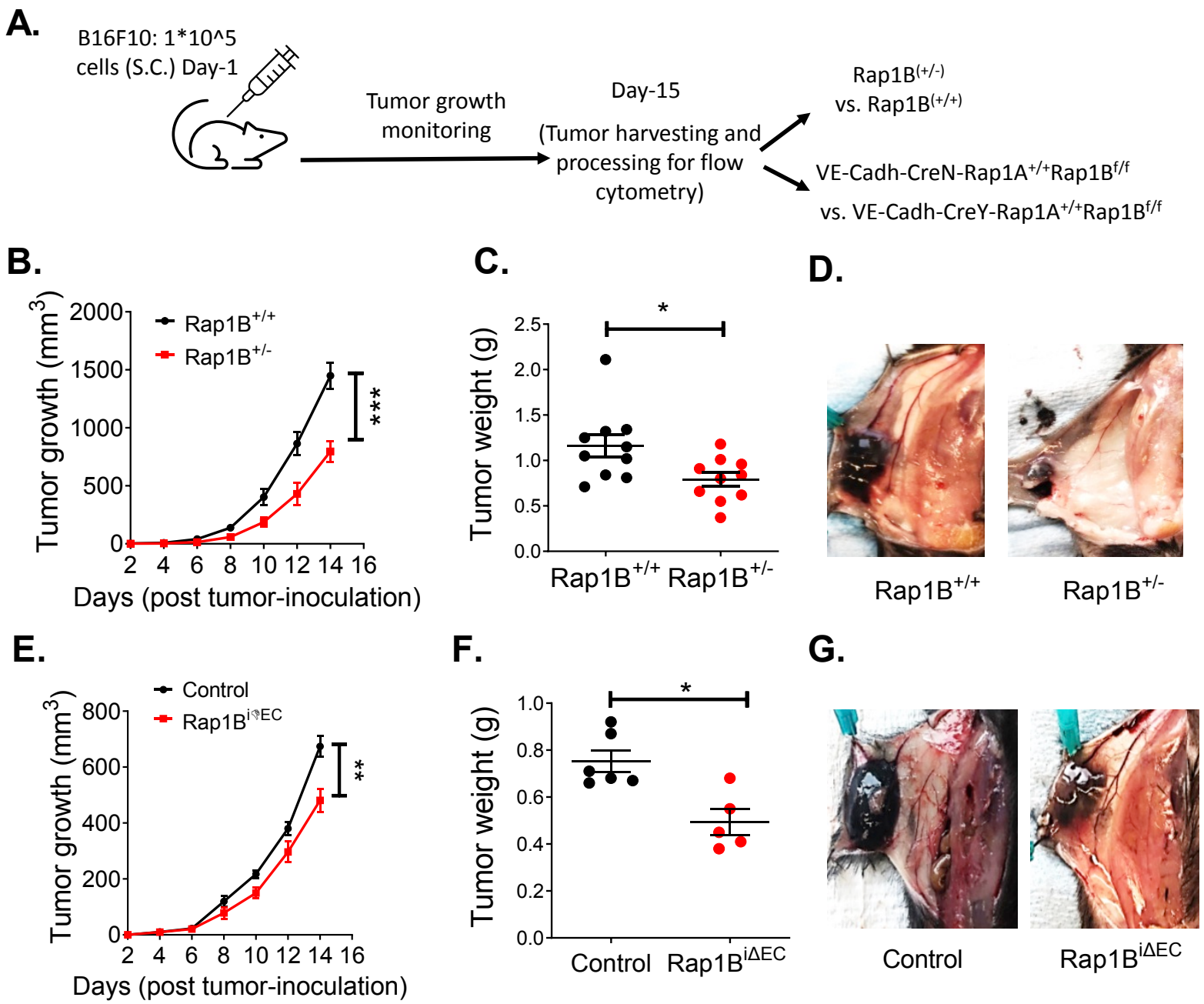

Figure 1. Global and EC-specific Rap1B deletion restricts tumor growth in vivo.
(A) A schematic diagram of melanoma induction in global Rap1B-deficient mice, $Rap1B^{+/-}$, or EC-specific Rap1B knockouts, $Rap1B^{i\Delta EC}$. Tumor growth kinetics **(B),** tumor weight at day 15 **(C)** and representative photographs of melanoma growth **(D)** in $Rap1B^{+/-}$ (n=10) vs. $Rap1B^{+/+}$ (n=10) mice. Tumor growth kinetics **(E)**, tumor weights **(F)** and representative photographs of melanoma growth **(G)** in $Rap1B^{i\Delta EC}$ (n=5) vs. Cre-negative control mice (n=6). Data represent mean ± SEM. *, $P < 0.05$ **, $P < 0.01$, ***, $P < 0.001$, Student's *t* test. Data and statistical outputs are available in *Figure 1-source data 1* file.

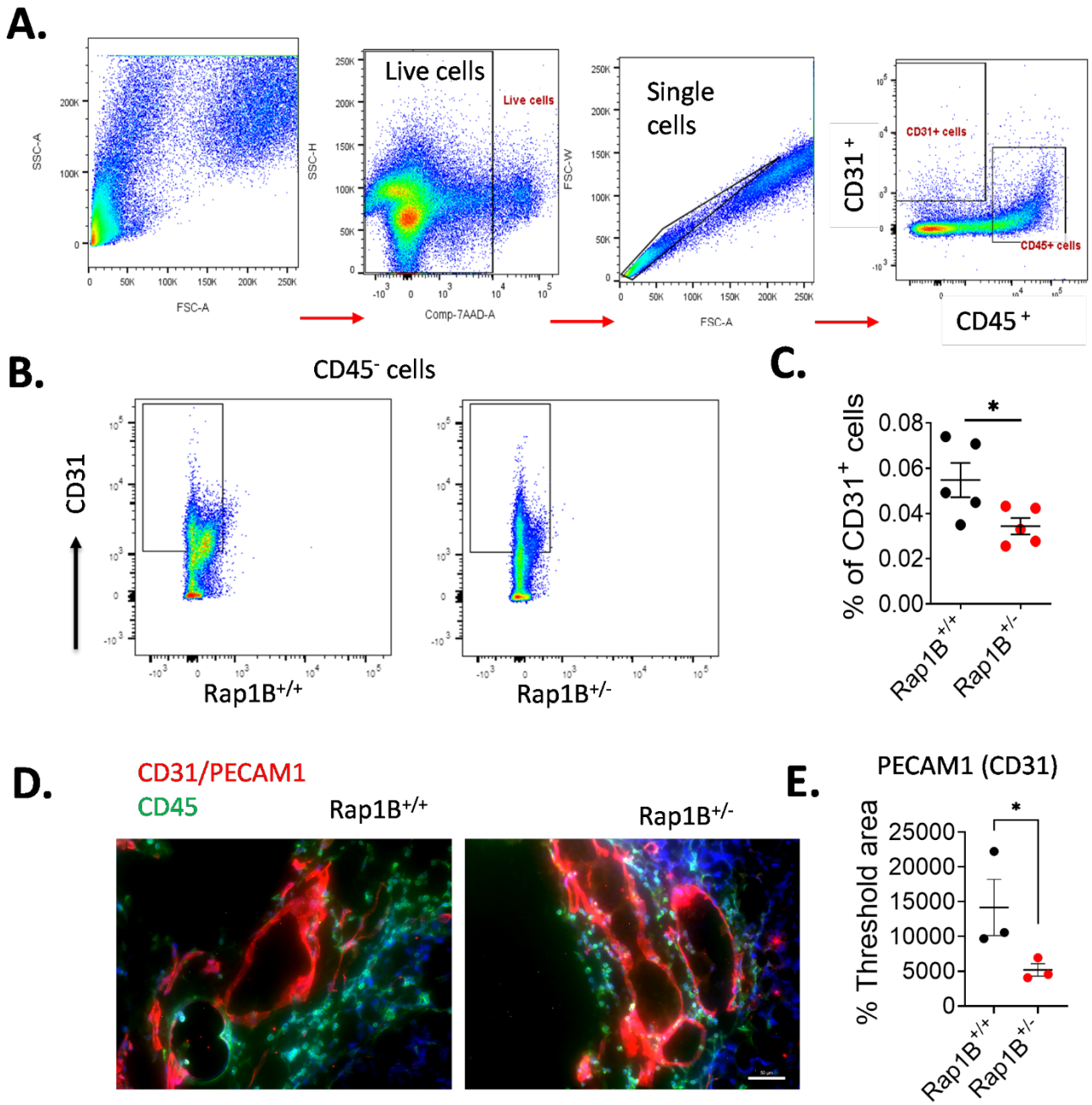

Figure 1- figure supplement 1. Reduced CD31⁺ endothelial cells in Rap1B$^{+/-}$ tumors. (**A**). Gating strategy for endothelial cells (CD31⁺) and leukocytes (CD45⁺) using stained single-cell suspension from the harvested tumors. Representative plots from a control tumor are shown. One million events were acquired on BD FACS-diva (LSR II-Green) using single-cell suspension from the harvested tumors. Viable, 7-AAD-negative cells were identified, and cell doublets were discriminated by their SSC and FSC characteristics. Single cells were further gated for leukocytes (CD45⁺/CD31⁻) and endothelial cells (CD31⁺/CD45⁻). (**B**) Decreased number of tumor endothelial cells (CD31⁺/CD45⁻) isolated from Rap1B$^{+/-}$ mice vs. control, shown as % of gated single cells (**C** *, $P < 0.05$). Data are presented as the mean ± S.E.M. n = 5 mice per group, student's *t* test. (**D**) Typical immunofluorescent staining of CD45⁺ cells (green) and CD31⁺ endothelial cells (red) in tumor sections. (**E**) CD31⁺ endothelial cells quantification demonstrates a significant decrease in ECs in tumor sections in Rap1B$^{+/-}$, vs. control group (*, $P < 0.05$). n = 3 mice per group, Student's *t* test. Data and statistical outputs are available in *Figure 1 – figure supplement 1-source data 1* file.

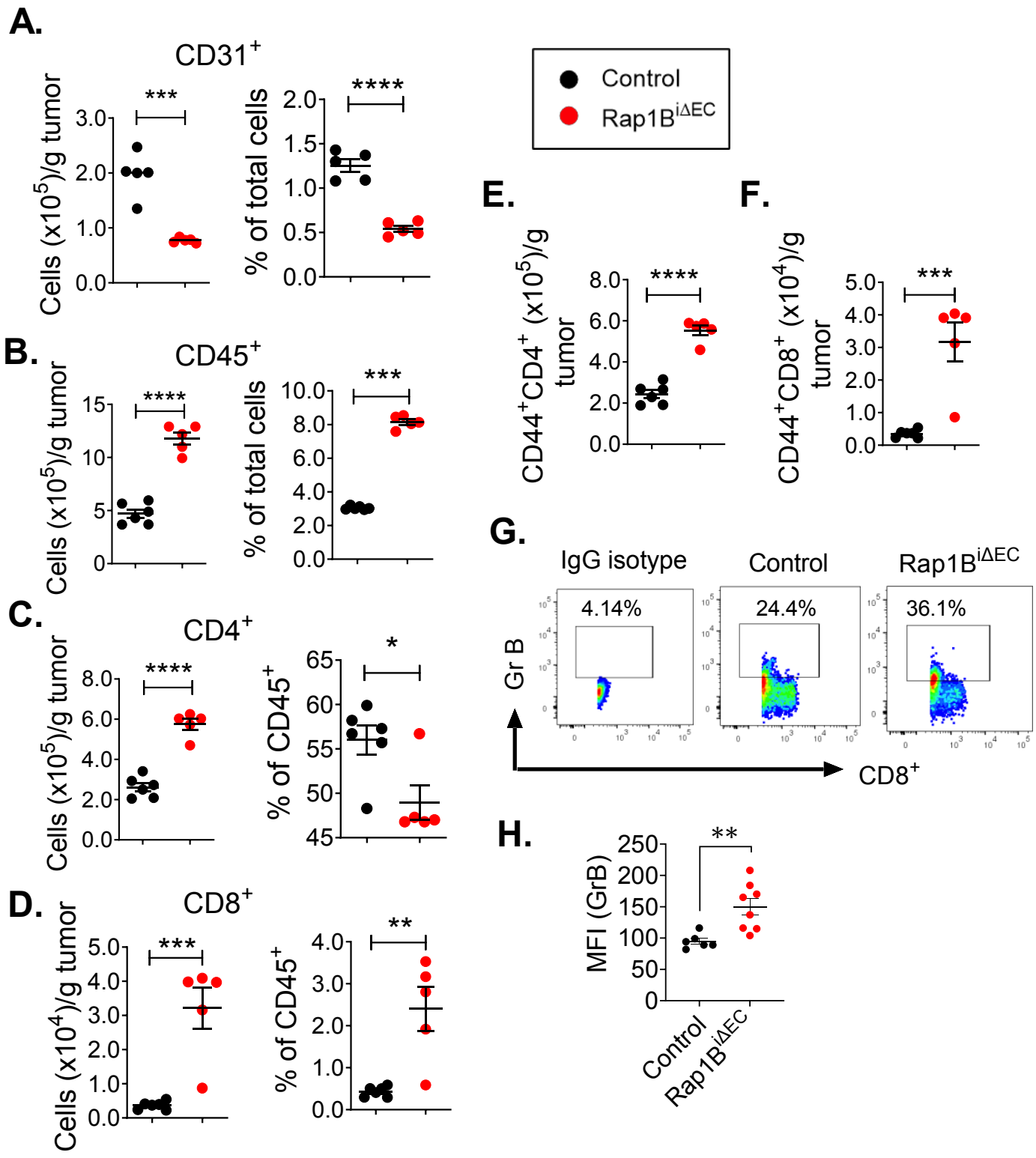

Figure 2. Endothelial Rap1B restricts tumor T-cell infiltration. (A-D) Endothelial Rap1B-deficiency alters TME cellularity. Flow cytometry analysis of single cell suspensions from tumors stained with cell-type specific markers demonstrate decreased endothelial cell numbers ($CD31^{+}$, **A),** and increased $CD45^{+}$ cells **(B)** in $Rap1B^{i\Delta EC}$ (n=5) vs. control mice (n=5). Gating strategy shown in Supplementary Fig. S1. $CD4^{+}$ T cells **(C)** and $CD8^{+}$ T cells **(D)** selected as shown in gating scheme in Supplementary Fig. S3. (**E-H**) **Elevated T cell activation in $Rap1B^{i\Delta EC}$ vs. control mice.** Surface expression of T-cell activation marker CD44 in $CD4^{+}$T **(E)** and $CD8^{+}$T **(F)** cells in $Rap1B^{i\Delta EC}$ (n=5) and control mice (n=6) tumors. **(G-H)** Representative FACS plots (**G**) and quantification of median fluorescence intensity, (MFI, **H**) of intracellular staining for granzyme B (GrB) in tumor $CD8^{+}$T cells from $Rap1B^{i\Delta EC}$ (n=8) and control mice (n=5). Data represent mean ± SEM. *, $P < 0.05$ **, $P < 0.01$, ***, $P < 0.001$, Student's t-test. Data and statistical outputs are available in *Figure 2-source data 1* file.

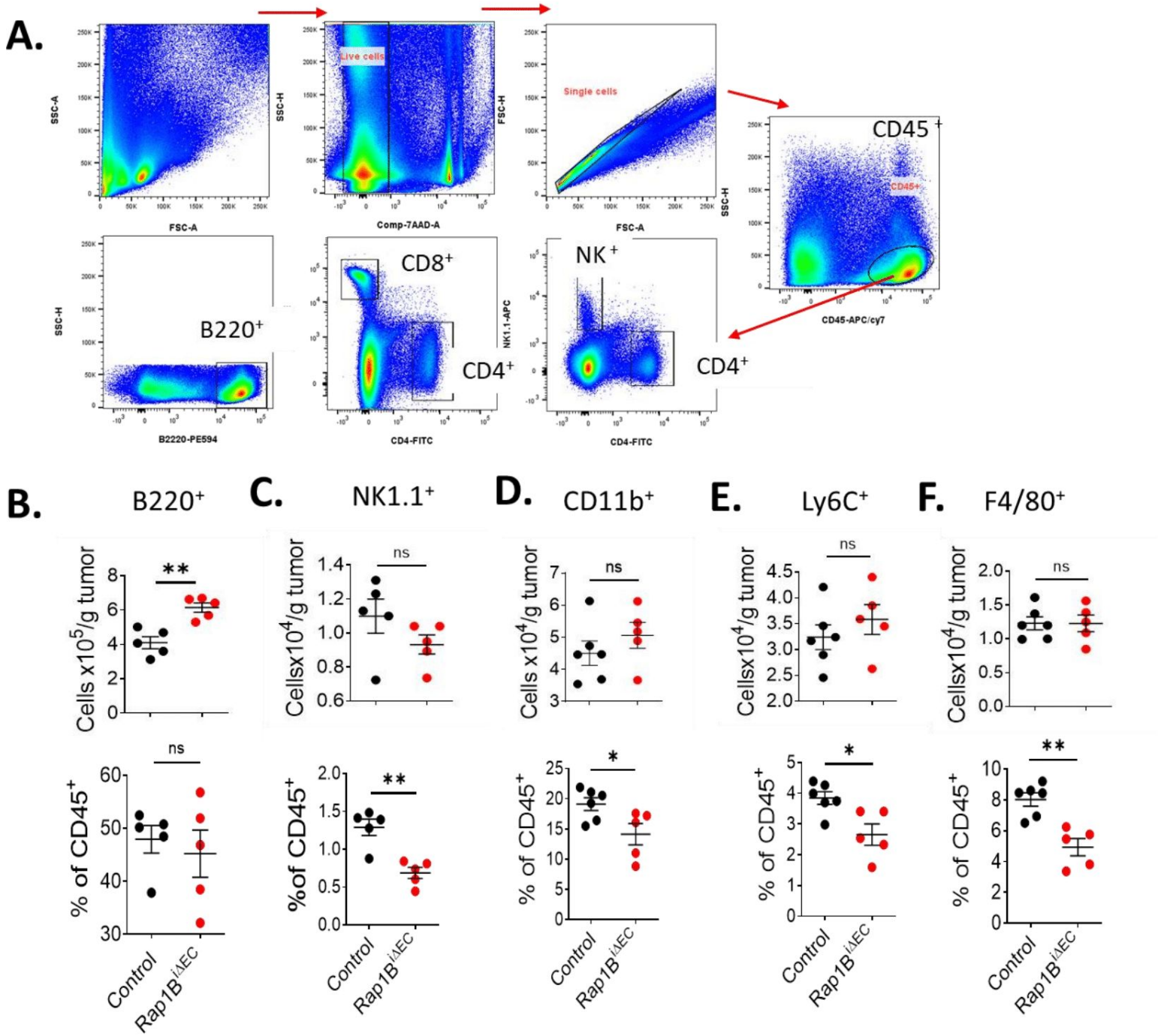

Figure 2-figure supplement 1. EC-specific Rap1B deletion alters recruitment of tumor-infiltrating lymphocytes (TIL). (**A**) Gating and selection of immune cell types from tumor single-cell suspensions. Representative plots from a control tumor are shown. One million events were acquired on BD FACS-diva (LSR II-Green) using single-cell suspension from the harvested tumors. Single cells were used to identify CD45$^+$ leukocytes, which were further gated using marker-specific antibodies against NK1.1 (natural killer cells), CD4, CD8 and B220 B-cells. **B-F.** Quantitation of cell populations: **(B)** B cells (B220$^+$), **(C)** natural killer cells (NK1.1$^+$), **(D)** myeloid cells (CD11b$^+$), **(E)** monocytes (Ly6C$^+$) and **(F)** macrophage (F4/80$^+$) in single-cell suspension of tumors from Rap1B$^{i\Delta EC}$ or control mice. Data are presented as the mean ± S.E.M. *, $P < 0.05$. n = 5 mice per group, Student's *t* test. Data and statistical outputs are available in *Figure 2– figure supplement 1-source data 1* file.

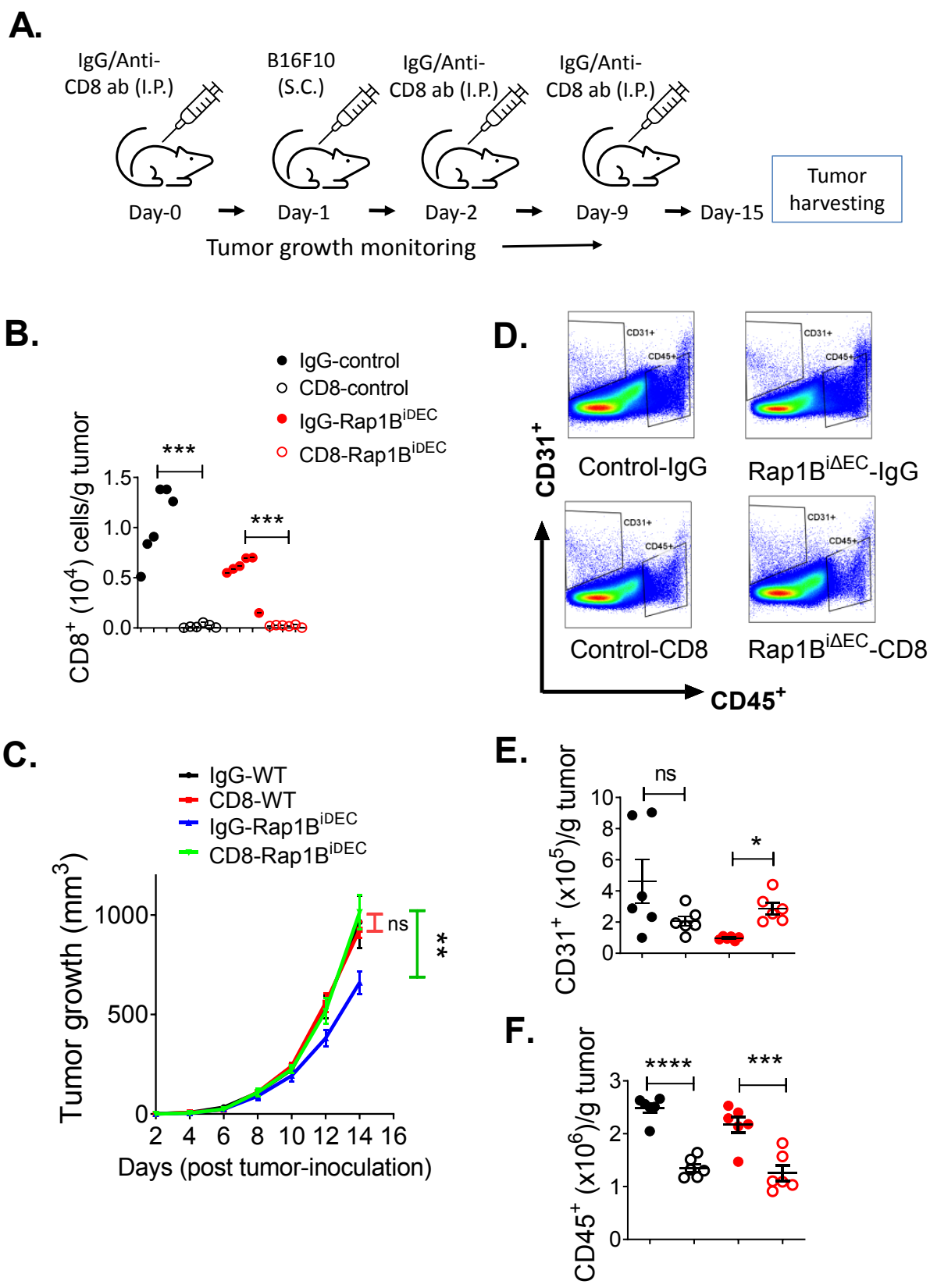

Figure 3. Depletion of CD8⁺ T cells normalizes tumor growth in Rap1B$^{i\Delta EC}$ mice. (A) Schematic diagram of antibody treatment (intraperitoneal, I.P. injection) and melanoma induction (subcutaneous, S.C. injection). **(B)** Quantification of CD8⁺ T cells demonstrates highly efficient cell depletion in with anti-CD8 antibody or IgG isotype control. **(C)** Tumor growth kinetics in Rap1B$^{i\Delta EC}$ vs. Cre-negative control treated with anti-CD8 . **(D)** Gating scheme and quantification of CD31⁺ ECs **(E)** and CD45⁺ cells **(F).** Data are presented as the mean ± S.E.M (n=6 per group). *, P < 0.05, **, P < 0.01, ***, P < 0.001, Panels B, C, F: one-way ANOVA with Tukey's post hoc test. Panel E: Student's t-test. Data and statistical outputs are available in *Figure 3-source data 1* file.

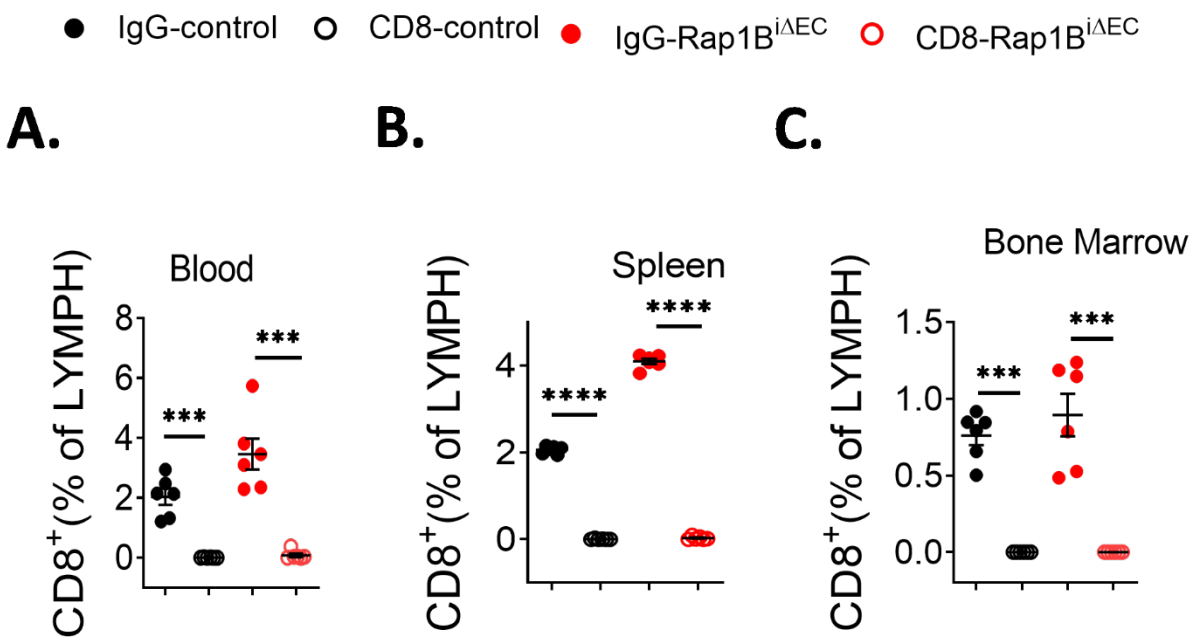

Figure 3 – figure supplement 1. Efficiency of CD8⁺ T cell depletion in specific tissue compartments.
Peripheral blood cells **(A)**, spleen cells **(B)** and bone marrow cells (**C)** were stained with Very CD8 mAb. Flow analysis showing drastic depletion of CD8⁺ cells in all tissue compartment. IgG isotype control has no significant modulation on T cell. Data are presented as the mean ± S.E.M. ***, P < 0.001, ****, P < 0.0001. n = 6 mice per group, one-way ANOVA with Tukey's multiple comparisons post hoc test. Data and statistical outputs are available in *Figure 3 – figure supplement 1-source data 1* file.

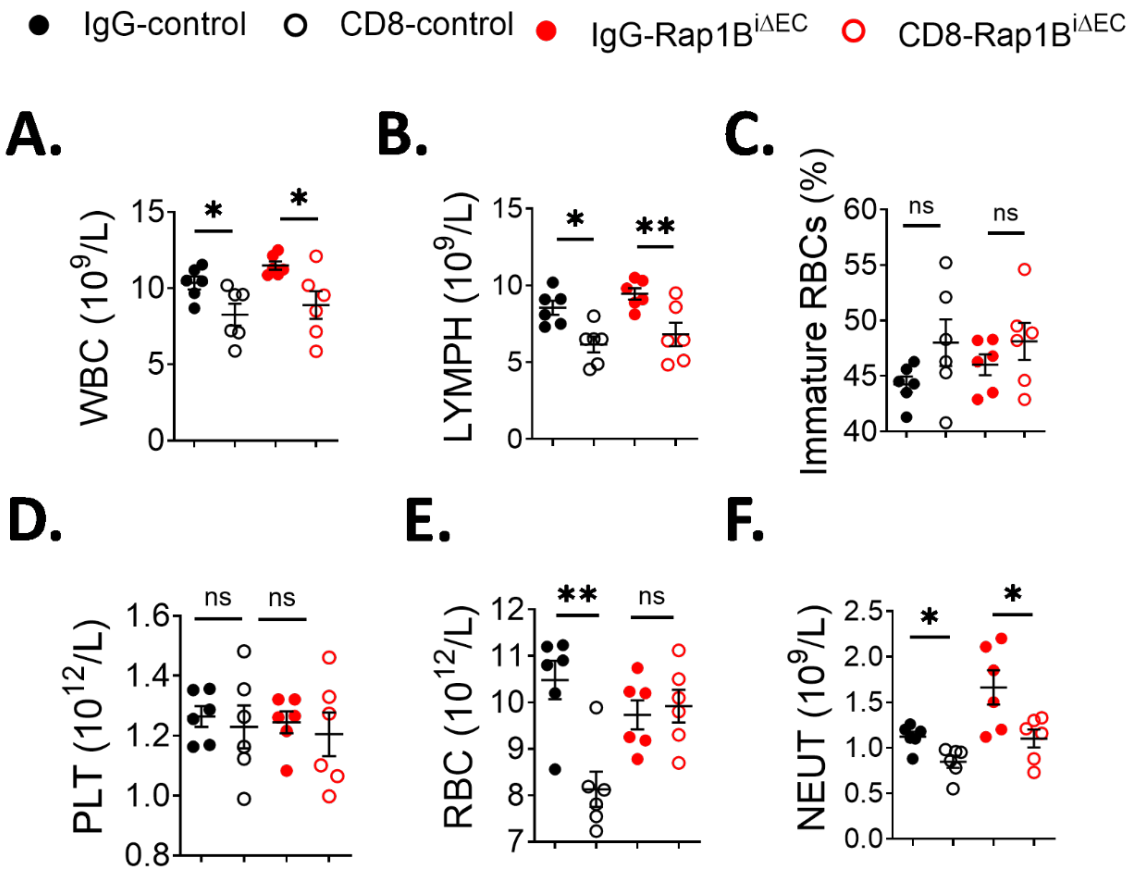

Figure 3 − figure supplement 2. Hematological (CBC) analysis in control and Rap1B$^{i\Delta EC}$ mice after CD8$^+$ T cell depletion. Whole blood (13 µl per mouse) was collected into anticoagulant (1:10) using capillary tubes (StatSpin® Microhematocrit Tubes, VWR). The blood samples were immediately analyzed using an automated Hematology blood analyzer (Sysmex XN-1000™). CBC counts: **(A)** White blood cells (WBC) 10^9/L; **(B)** lymphocyte (LYMPH) 10^9/L. **(C)** Immature (young) RBC fraction, as measured by % of high fluorescence reticulocyte (HFR), **(D)** Platelets (PLT) 10^{12}/L, **(E)** Red blood cells (RBC) 10^{12}/L, and **(F)** Neutrophils (NEUT). Data are presented as the mean ± S.E.M. *, $P < 0.05$, **, $P < 0.01$. n = 6 mice per group, one-way ANOVA with Tukey's multiple comparisons post hoc test. Data and statistical outputs are available in *Figure 3 – figure supplement 2-source data 1* file.

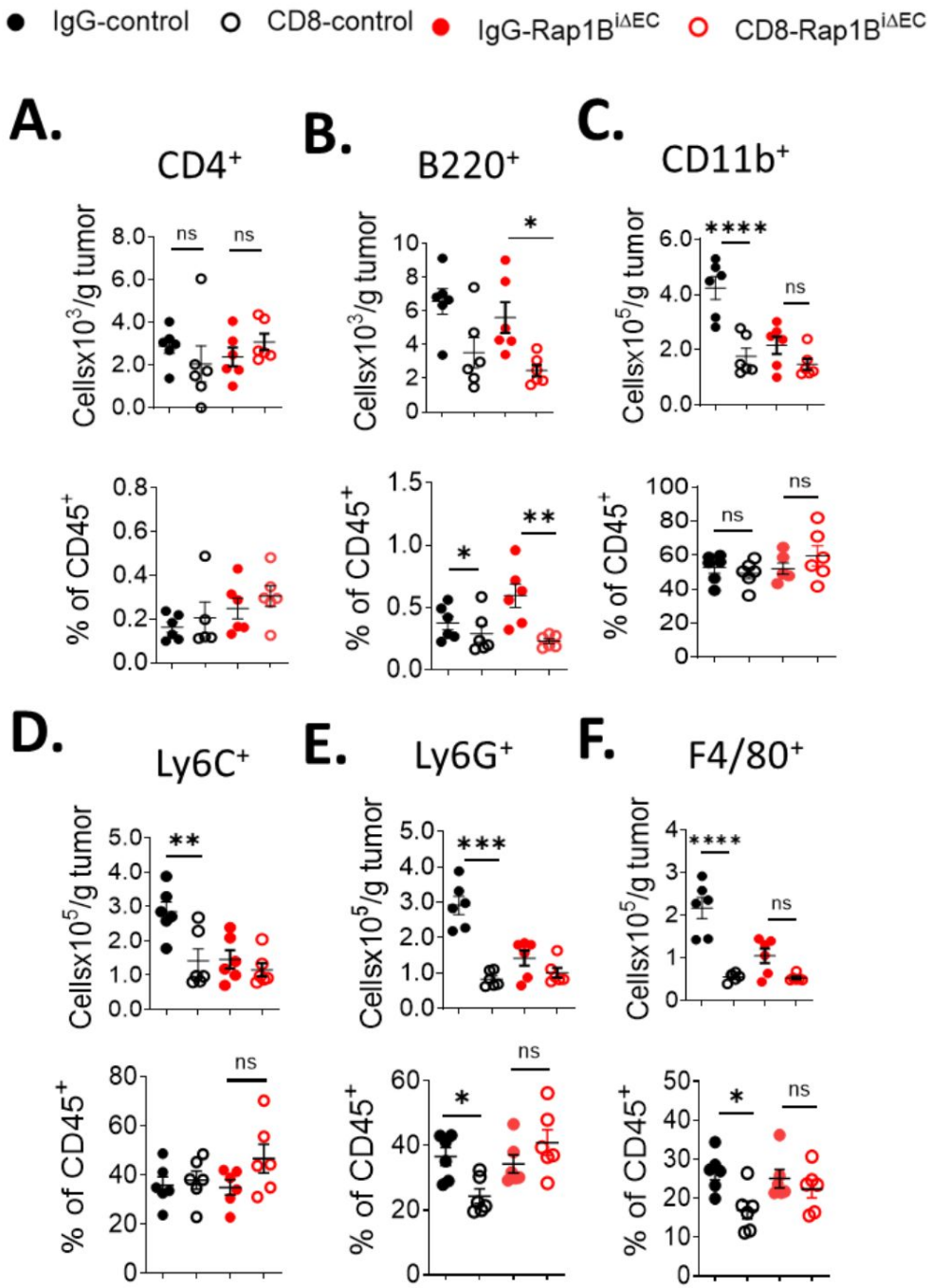

Figure 3 − figure supplement 3. Effect of CD8$^+$ T-cell depletion on tumor-infiltrating lymphocytes (TIL) in control and Rap1B$^{i\Delta EC}$ mice. Immunophenotypic examination showing quantitation of **(A)** CD4$^+$T cells, **(B)** B cells (B220$^+$), **(C)** myeloid cells (CD11b$^+$), **(D)** monocytes (Ly6C$^+$), **(E)** neutrophils (Ly6G$^+$) and **(F)** macrophage (F4/80$^+$) in Rap1B$^{i\Delta EC}$/control mice treated with either IgG isotope or CD8 mAb. Data are presented as the mean ± S.E.M. *, P < 0.05, **, P < 0.01. n = 6 mice per group, one-way ANOVA with Tukey's multiple comparisons post hoc test. Data and statistical outputs are available in *Figure 3 – figure supplement 3-source data 1* file.

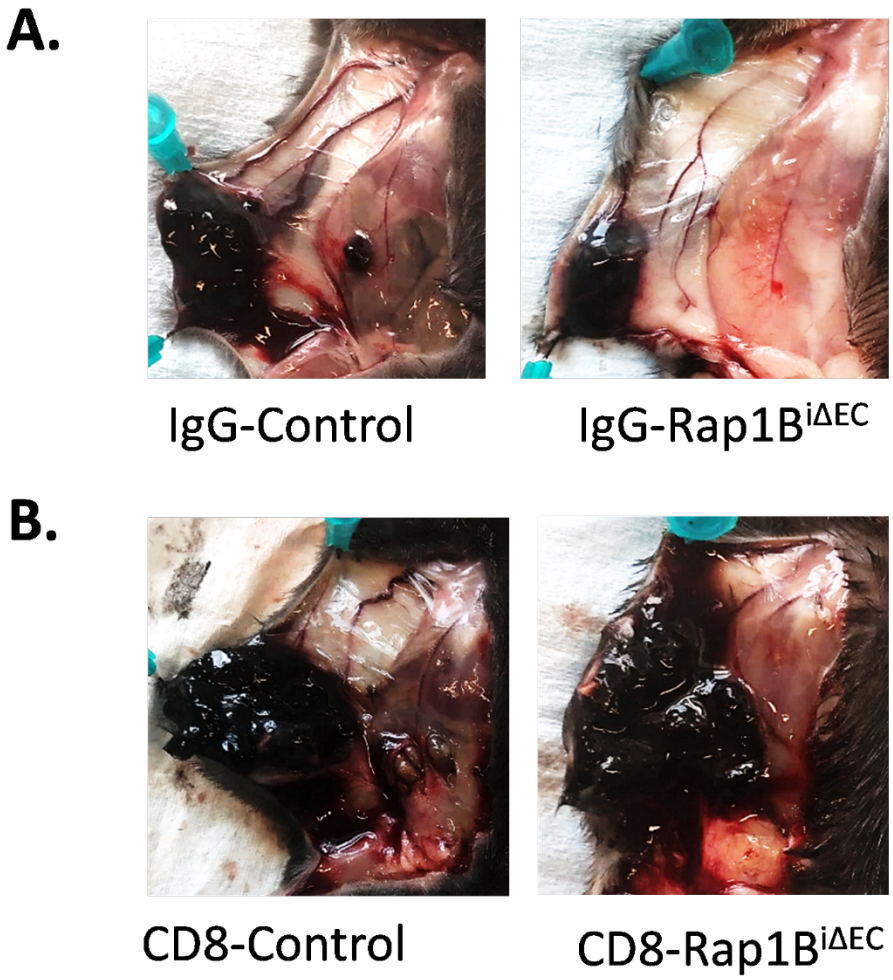

Figure 3 – figure supplement 4. Depletion of CD8^{+} T-cells normalizes tumor growth in Rap1B$^{i\Delta EC}$ mice. Representative photographs showing pattern of tumor growth in Rap1B$^{i\Delta EC}$/control mice treated with either IgG isotope or CD8 mAb. **(A)** IgG isotope has no effect on tumor growth in control group. **(B)** CD8^{+} T cell depletion significantly rescued tumor reduction in Rap1B$^{i\Delta EC}$ mice group.

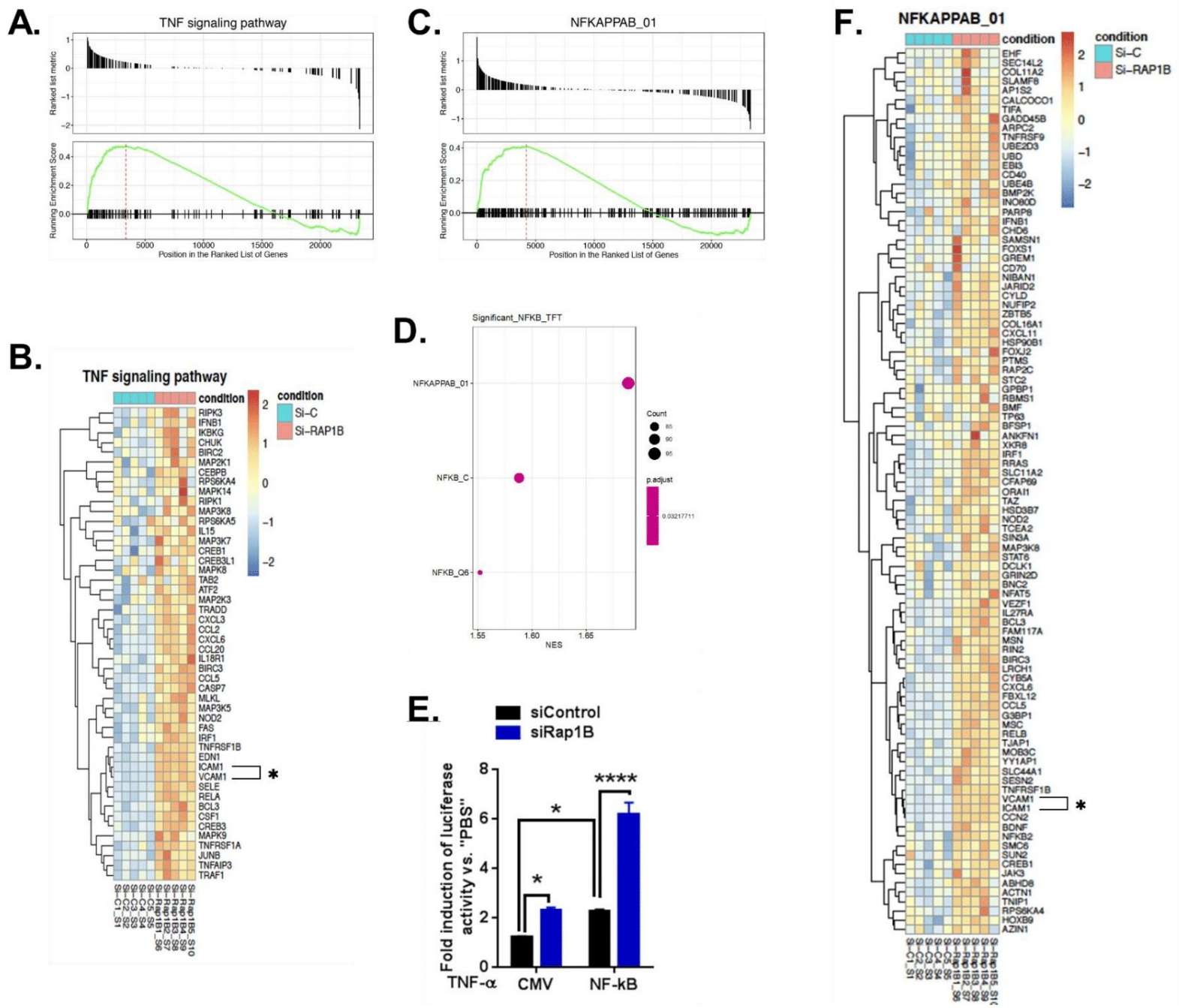

Figure 4. Endothelial Rap1B restricts TNF-α induced NFκB activation.
Increased TNF-α signaling and NFκB transcription detected by bulk RNA sequencing of TNF-α-treated siRap1B and siControl Ecs. **(A)** Gene set enrichment analysis (GSEA) of genes in TNF-α signaling pathway upregulated in siRap1B vs. siControl. **(B)** Heatmap of selected genes from TNF-α signaling pathway. **(C)** GSEA of NFκB signaling pathway. **(D)** Transcriptional activation of NFκB in siRap1B ECs. **(E)** TNF-α-induced NFκB activity determined by luciferase assay in cells transfected with NF-κB reporter construct or a control vector (CMV). Values shown as mean fold change vs. PBS-treated cells . Error bars represent mean ± SD (n = 6). *, P < 0.05, ****, P < 0.0005. One-way ANOVA followed by Tukey's multiple comparisons test. **(F)** Heatmap of selected genes from NFκB pathway. (n = 5 separate EC sets per group). Link to sequence data deposited within NCBI GEO is available in *Figure 4-source data 1* file. Data and statistical outputs for panel E are available in *Figure 4-source data 2* file.

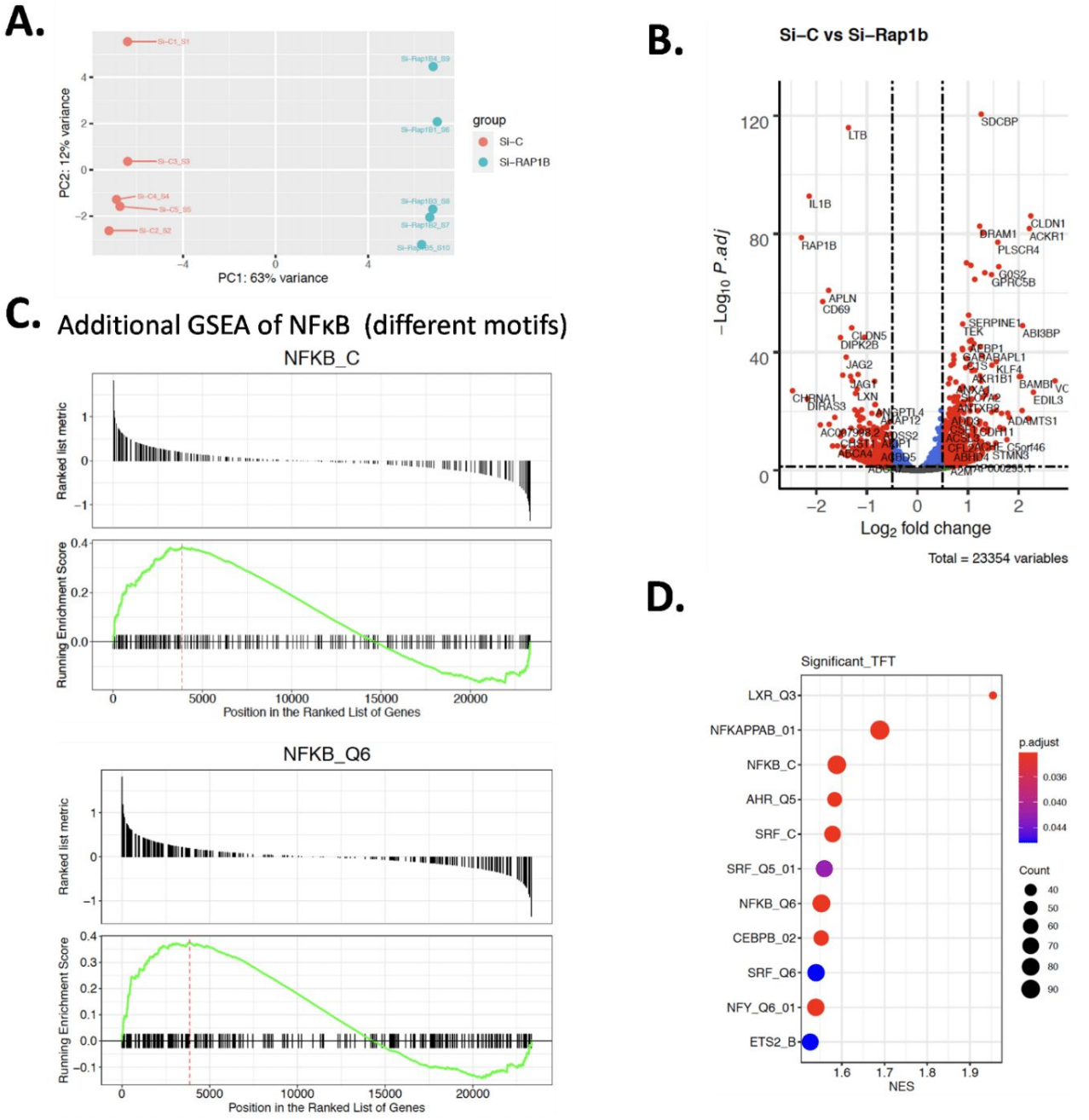

Figure 4 − figure supplement 1. Transcriptomic analysis of TNF-α-stimulated siControl and siRap1B ECs. (A) Principal component analysis of samples. (**B**) Volcano plot of differential gene expression, the top 50 significantly differentially expressed genes are labeled. (**C**) Gene set enrichment analyses (GSEA) of NFκB target genes. (**D**) Dot plot of top significantly enriched transcription factors by GSEA (n = 5). Link to sequence data deposited within NCBI GEO is available in *Figure 4-source data 1* file.

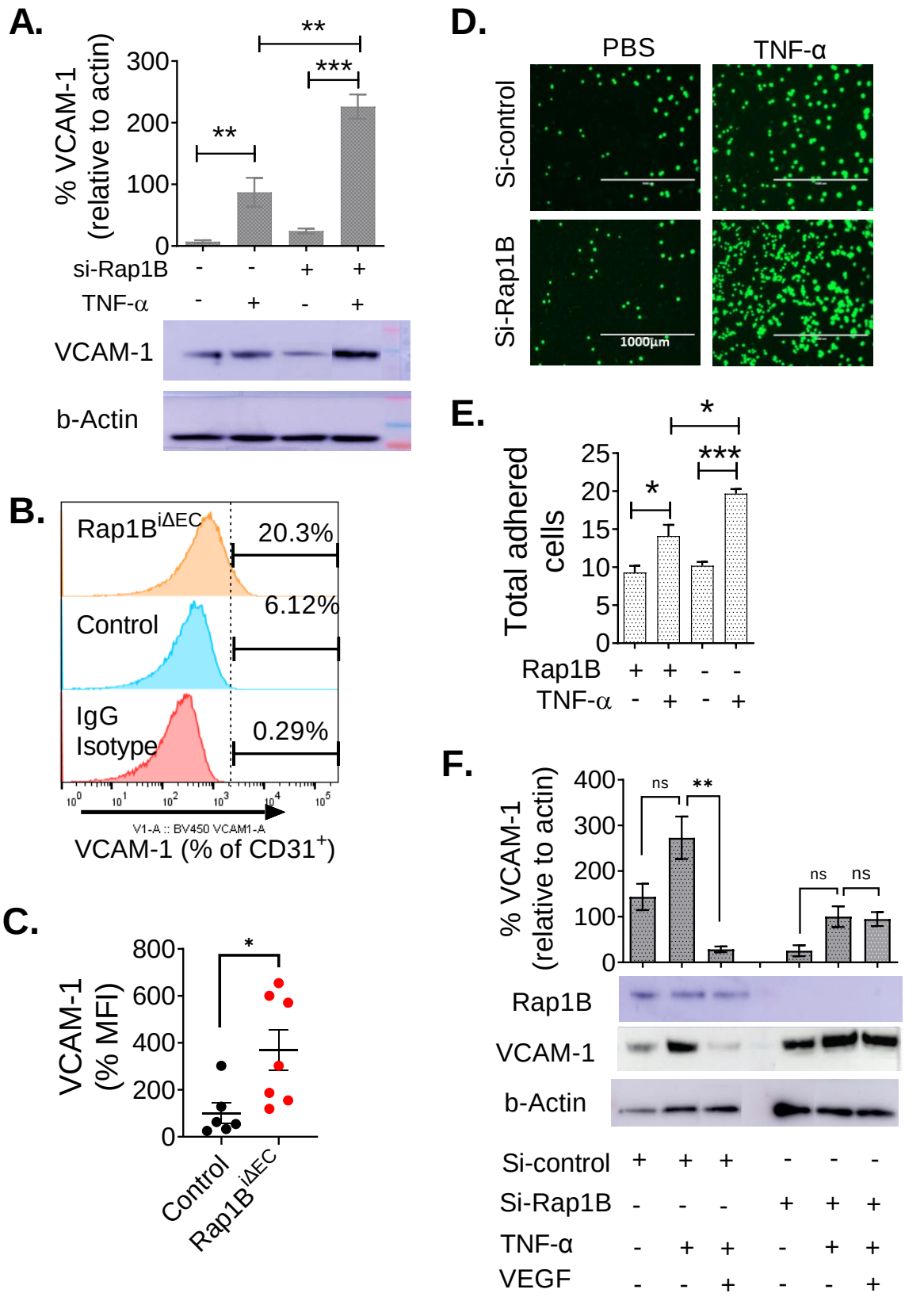

Figure 5. Endothelial Rap1B restricts proinflammatory CAM expression, mediates VEGF signaling. (A) Top: Densitometry of TNFα-induced VCAM-1 expression, normalized to actin, in siControl- or siRap1B- transfected HUVECs. Bottom: representative Western blot. Original images are available in *Figure 5-source data 1* file. **(B, C)** VCAM-1 expression in tumor ECs ($CD31^+$ cells): representative flow cytometry histogram (**B**) and median fluorescence intensity (MFI) (**C**). n ≥ 5 mice per group, **(D, E)** EC-Rap1B deficiency leads to increased leukocyte adhesion in vitro. Representative image (**D**) and quantification (**E**) of Calcein-AM-labeled Jurkat cells adhering to siRap1B and siControl ECs following TNF-α treatment 12 hours. Adhesion efficiency is expressed as Jurkat cells bound/10,000 plated. (**F**) VEGF treatment inhibits TNF-α-induced CAM expression in siControl but not in siRap1B ECs. Densitometry (top) and representative Western blot (bottom) are shown. Original images are available in *Figure 5-source data 2* file. Data shown are mean ± S.E.M. *, $P < 0.05$, **, $P < 0.01$, ***, $P < 0.001$, Panels A, E, F: one-way ANOVA followed by Tukey's multiple comparisons test. Panel C: Student's t-test. Data and statistical outputs are available in *Figure 5-source data 3* file.

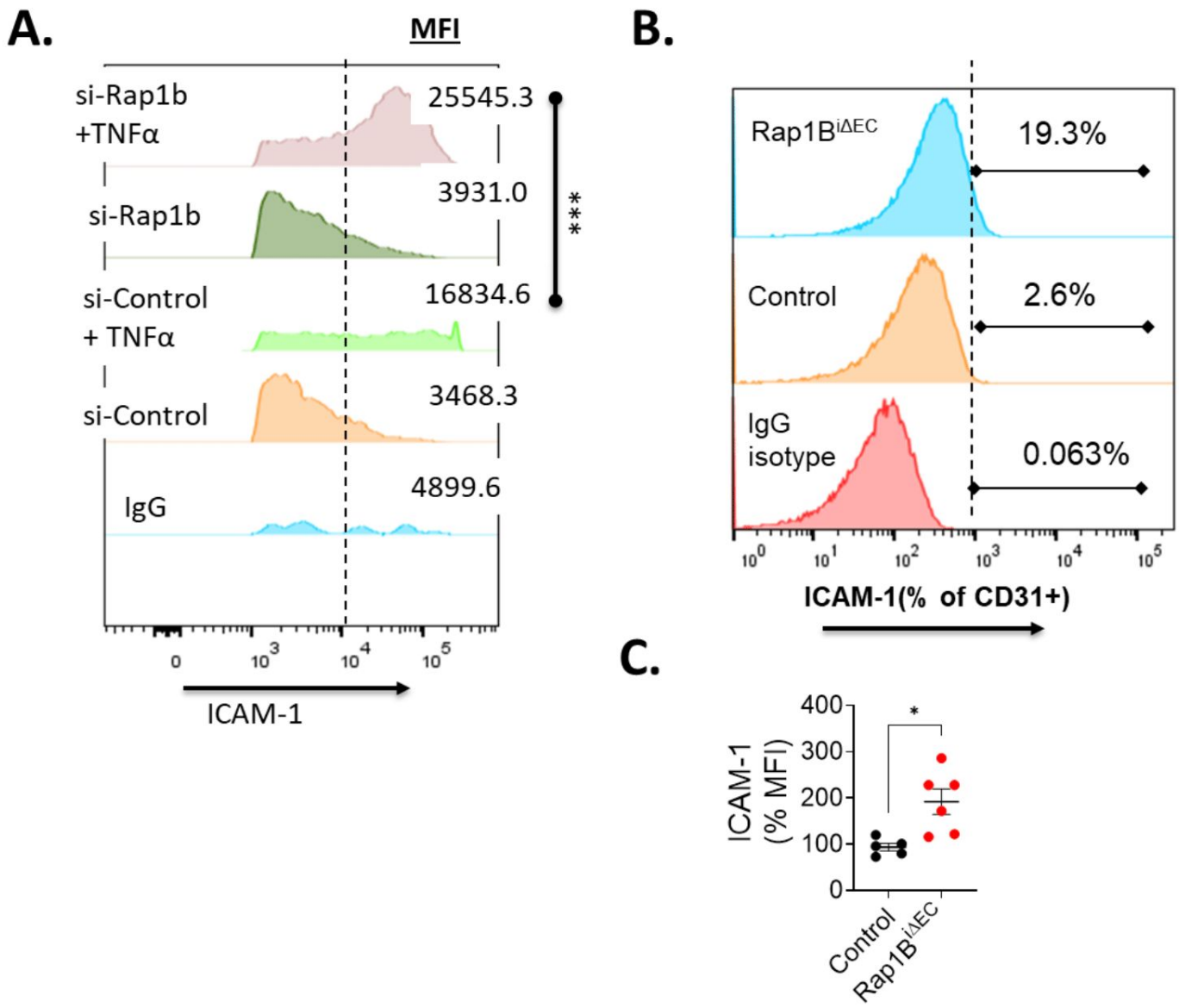

Figure 5 – figure supplement 1. Elevated ICAM-1 surface expression in Rap1B-deficient tumor ECs and HUVECs. (A) Flow cytometric analysis of ICAM-1 expression on siRap1B and siControl HUVEC cells. (**B**) Flow cytometric analysis of ICAM-1 expression on tumor ECs from Rap1B$^{i\Delta EC}$ and control mice**:** representative flow cytometry histogram and median fluorescence intensity (MFI) plot (**C**). Data are presented as the mean ± S.E.M. **, P < 0.01, Student's t test. Data and statistical outputs are available in *Figure 5 – figure supplement 1-source data 1* file.

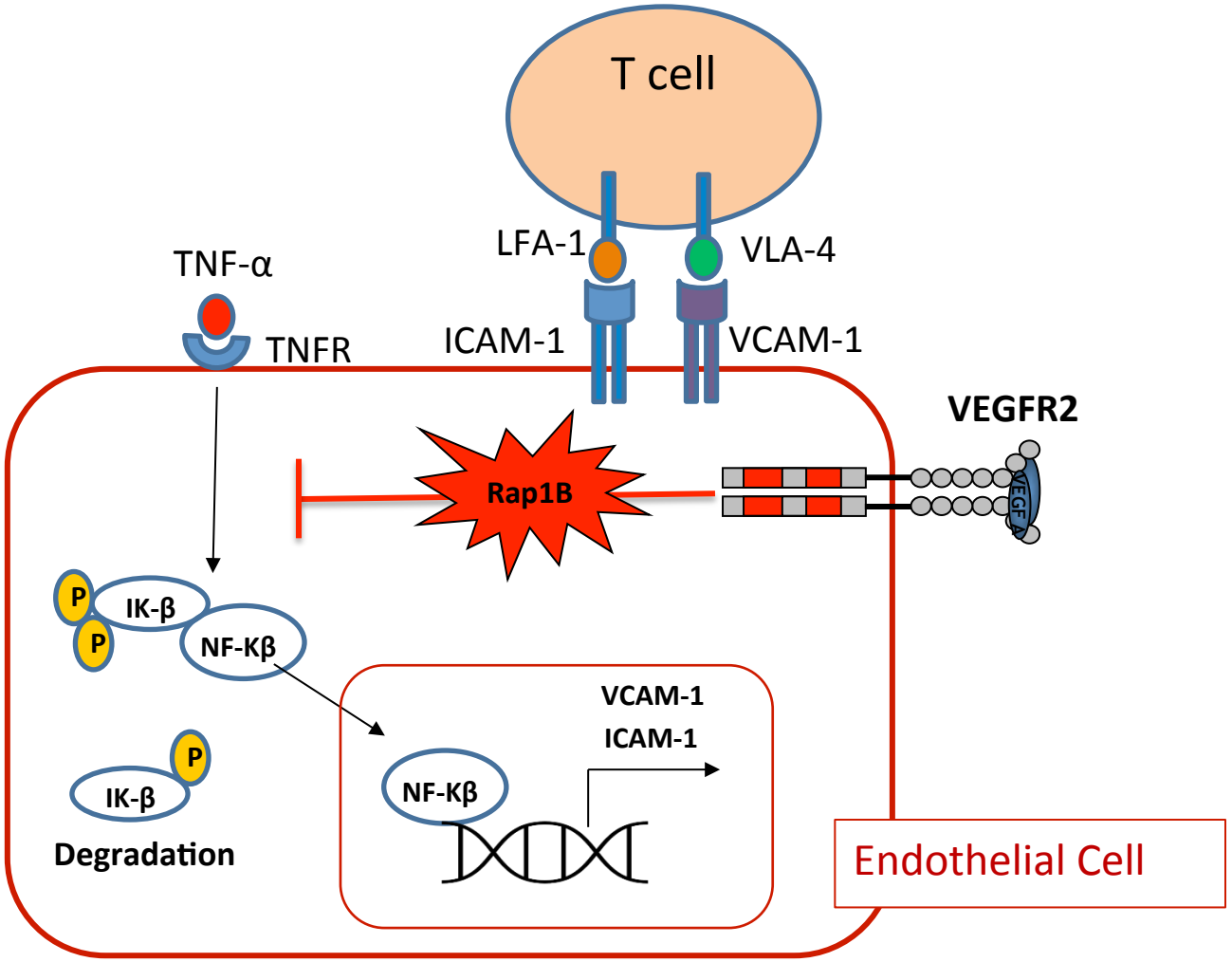

Figure 6. Endothelial Rap1B conveys VEGF suppression of immune reactivity – proposed mechanism. Under normal conditions Rap1 suppresses cytokine-induced CAM expression, limiting T-cell adhesion and recruitment. In proangiogenic conditions of TME, VEGF signaling, mediated by Rap1B, suppresses this endothelial immune response.